

Extreme Electronic Modulation of the Cofacial Porphyrin Structural Motif

James T. Fletcher and Michael J. Therien*

Contribution from the Department of Chemistry, University of Pennsylvania,
231 South 34th Street, Philadelphia, Pennsylvania 19104-6323

Received November 6, 2001

Abstract: The synthesis, electrochemistry, and optical spectroscopy of an extensive series of cofacial bis[(porphinato)zinc(II)] compounds are reported. These species were synthesized using sequential palladium-catalyzed cross-coupling and cobalt-mediated [2+2+2] cycloaddition reactions. This modular methodology enables facile control of the nature of macrocycle-to-macrocycle connectivity and allows unprecedented modulation of the redox properties of face-to-face porphyrin species. We report the synthesis of 5,6-bis-[(5',5''-10',20'-bis[4-(3-methoxy-3-methylbutoxy)phenyl]porphinato)zinc(II)]indane (**1**), 5,6-bis-[(2'-5',10',15',20'-tetraphenylporphinato)zinc(II)]indane (**2**), 5-[(2'-5',10',15',20'-tetraphenylporphinato)zinc(II)]-6-[(5''-10'',20''-bis[4-(3-methoxy-3-methylbutoxy)phenyl]porphinato)zinc(II)]indane (**3**), 5-[(2'-5',10',15',20'-tetrakis(trifluoromethyl)porphinato)zinc(II)]-6-[(5''-10'',20''-bis[4-(3-methoxy-3-methylbutoxy)phenyl]porphinato)zinc(II)]indane (**4**), 5-(2'-5',10',15',20'-[tetrakis(trifluoromethyl)porphinato]zinc(II))-6-[(2''-5'',10'',15'',20''-tetraphenylporphinato)zinc(II)]indane (**5**), 5,6-bis-[(2'-5',15'-diphenyl-10',20''-(trifluoromethyl)porphinato)zinc(II)]indane (**6**), and 5,6-bis-[(2'-5',10',15',20'-tetrakis(trifluoromethyl)porphinato)zinc(II)]indane (**7**); **4**–**7** define the first examples of cofacial bis[(porphinato)metal] compounds in which σ -electron-withdrawing perfluoroalkyl groups serve as macrocycle substituents, while **2**, **6**, and **7** constitute the first such structures that possess a β -to- β linkage topology. Cyclic voltammetric studies show that the electrochemically determined HOMO and LUMO energy levels of these cofacial bis(porphinato) complexes can be lowered by 780 and 945 mV, respectively, relative to the archetypal members of this class of compounds; importantly, these orbital energy levels can be modulated over well-defined increments throughout these wide potentiometric domains. Analyses of these cofacial bis[(porphinato)metal] potentiometric data, in terms of the absolute and relative frontier orbital energies of their constituent [porphinato]zinc(II) building blocks, as well as the nature of macrocycle-to-macrocycle connectivity, provide predictive electronic structural models that rationalize the redox behavior of these species.

Introduction

Though mastered by Nature, the design of biomimetic catalysts satisfying the thermodynamic and kinetic requirements necessary for small-molecule multielectron transformations remains challenging. Pioneering studies involving cofacial metalodiporphyrins have provided valuable mechanistic insight regarding a variety of small-molecule reductive and oxidative transformations that require respectively pairwise delivery or removal of electrons.^{1–15} Despite the established catalytic utility

of these species, demanding syntheses coupled with limited tools to modulate the electronic properties of these systems have impeded the syntheses of more elaborate versions of the structural motif.^{16–22}

- (1) Collman, J. P.; Elliott, C. M.; Halbert, T. R.; Tovrog, B. S. *Proc. Natl. Acad. Sci. U.S.A.* **1977**, *74*, 18–22.
- (2) Chang, C. K.; Kuo, M.-S.; Wang, C.-B. *J. Heterocycl. Chem.* **1977**, *14*, 943–945.
- (3) Kagan, N. E.; Mauzerall, D.; Merrifield, R. B. *J. Am. Chem. Soc.* **1977**, *99*, 5484–5486.
- (4) Collman, J. P.; Denisevich, P.; Konai, Y.; Marrocco, M.; Koval, C.; Anson, F. C. *J. Am. Chem. Soc.* **1980**, *102*, 6027–6036.
- (5) Chang, C. K.; Liu, H. Y.; Abdalmuhdi, I. *J. Am. Chem. Soc.* **1984**, *106*, 2725–2726.
- (6) Liu, H.-Y.; Abdalmuhdi, I.; Chang, C. K.; Anson, F. C. *J. Phys. Chem.* **1985**, *89*, 665–670.
- (7) Naruta, Y.; Maruyama, K. *J. Am. Chem. Soc.* **1991**, *113*, 3595–3596.
- (8) Karaman, R.; Jeon, S.; Almarsson, Ö.; Bruce, T. C. *J. Am. Chem. Soc.* **1992**, *114*, 4899–4905.
- (9) Collman, J. P.; Hutchison, J. E.; Ennis, M. S.; Lopez, M. A.; Guillard, R. *J. Am. Chem. Soc.* **1992**, *114*, 8074–8080.

- (10) Jeon, S.; Almarsson, Ö.; Karaman, R.; Blaskó, A.; Bruce, T. C. *Inorg. Chem.* **1993**, *32*, 2562–2569.
- (11) Collman, J. P.; Ha, Y.; Wagenknecht, P. S.; Lopez, M.-A.; Guillard, R. *J. Am. Chem. Soc.* **1993**, *115*, 9080–9088.
- (12) Collman, J. P.; Wagenknecht, P. S.; Hutchison, J. E. *Angew. Chem., Int. Ed. Engl.* **1994**, *33*, 1537–1554.
- (13) Naruta, Y.; Sasayama, M.; Sasaki, T. *Angew. Chem., Int. Ed. Engl.* **1994**, *33*, 1839–1841.
- (14) Naruta, Y.; Sasayama, M. *J. Chem. Soc., Chem. Commun.* **1994**, 2667–2668.
- (15) Collman, J. P.; Fish, H. T.; Wagenknecht, P. S.; Tyvoll, D. A.; Chng, L.-L.; Eberspacher, T. A.; Brauman, J. I.; Bacon, J. W.; Pignolet, L. H. *Inorg. Chem.* **1996**, *35*, 6746–6754.
- (16) Chang, C. K.; Abdalmuhdi, I. *J. Org. Chem.* **1983**, *48*, 5388–5390.
- (17) Chang, C. K.; Abdalmuhdi, I. *Angew. Chem., Int. Ed. Engl.* **1984**, *23*, 164–165.
- (18) Meier, H.; Kobuke, Y.; Kugimiya, S. *J. Chem. Soc., Chem. Commun.* **1989**, 923–924.
- (19) Osuka, A.; Nakajima, S.; Nagata, T.; Maruyama, K.; Toriumi, K. *Angew. Chem., Int. Ed. Engl.* **1991**, *30*, 582–584.
- (20) Collman, J. P.; Tyvoll, D. A.; Chng, L. L.; Fish, H. T. *J. Org. Chem.* **1995**, *60*, 1926–1931.
- (21) Deng, Y.; Chang, C. J.; Nocera, D. G. *J. Am. Chem. Soc.* **2000**, *122*, 410–411.
- (22) Chang, C. J.; Deng, Y.; Heyduk, A. F.; Chang, C. K.; Nocera, D. G. *Inorg. Chem.* **2000**, *39*, 959–966.

We recently established a new synthesis of 1,2-phenylene-bridged cofacial porphyrins²³ that exploits ethyne-bridged multiporphyrin precursors, and sequential Pd-catalyzed cross-coupling^{24–31} and metal-templated [2+2+2] cycloaddition reactions.^{32–34} We report herein the syntheses, optical spectroscopy, and electrochemistry of an extensive series of face-to-face bis[(porphinato)zinc(II)] compounds in which the nature of macrocycle–macrocycle connectivity, as well as the redox properties of their (porphinato)metal components, are varied systematically. Potentiometric data show that these engineering strategies enable unprecedented modulation of cofacial bis[(porphinato)metal] electronic structure; complimentary electronic structure analyses define simple models that rationalize the redox behavior of these systems in terms of the absolute and relative energy levels of the frontier orbitals of their respective (porphinato)zinc(II) building blocks.

Experimental Section

Inert atmosphere manipulations were carried out under nitrogen prepurified by passage through an O₂ scrubbing tower (Schweizerhall R3-11 catalyst) and a drying tower (Linde 3-Å molecular sieves). Air-sensitive solids were handled in a Braun 150-M glovebox. Standard Schlenk techniques were employed to manipulate air-sensitive solutions. A syringe pump was utilized to control reproducibly the time-dependent concentration of reagents in all metal-templated cycloaddition reactions.

Unless otherwise noted, all solvents utilized in this work were obtained from Fisher Scientific (HPLC grade) and distilled under nitrogen. Tetrahydrofuran and toluene were distilled from Na/benzophenone, and triethylamine was distilled from CaH₂; dioxane (anhydrous) was used as received from Aldrich. Pd₂(dba)₃, AsPh₃, and Co₂(CO)₈ were obtained from Strem. 1,6-Heptadiyne, TBAF, and ethynylbenzene were obtained from Aldrich. Trimethylsilylacetylene and triisopropylsilylacetylene were obtained from GFS Chemicals. Halogenated derivatives³⁵ of [5,10,15,20-tetrakis(trifluoromethyl)porphinato]zinc(II)^{36,37} and [5,15-bis(trifluoromethyl)-10,20-diphenylporphinato]zinc(II)³⁸ species were prepared similarly to methods reported previously; synthetic details are described in the Supporting Information.

Chromatographic purification (Silica 60, 230–400 mesh, EM Science) of all compounds was performed on the benchtop. Chemical shifts for ¹H NMR spectra are relative to residual protium (CDCl₃, δ 7.24 ppm), while those for ¹⁹F NMR spectra are referenced to fluorotrichloromethane (δ = 0.00 ppm).

Electronic spectra were recorded on an OLIS UV/visible/NIR spectrophotometry system that is based on the optics of a Carey 14 spectrophotometer. Cyclic voltammetric measurements were carried out with a PAR 273 electrochemical analyzer and a single-compartment

electrochemical cell. ¹H and ¹⁹F NMR experiments were performed respectively on 250- and 200-MHz Bruker instruments. MALDI-TOF mass spectroscopic data were obtained with a Perceptive Voyager DE instrument in the Laboratories of Dr. Virgil Percec (Department of Chemistry, University of Pennsylvania). Samples were prepared as micromolar solutions in THF, and dithranol (Aldrich) was utilized as the matrix.

General Procedure for the Preparation of Ethyne-Bridged Bis-[(porphinato)zinc(II)] Complexes.^{30,31} A 50-mL Schlenk tube was charged with a 2- or 5-ethynylporphyrin compound (1 equiv), a *meso*- or *β*-bromoporphyrin complex (1.2 equiv), Pd₂(dba)₃ (0.15 equiv), and AsPh₃ (1.2 equiv).³⁹ These reagents were dissolved in 5:1 THF/TEA and stirred for 3–26 h at 40 °C. Following evaporation of the solvent, the residue was purified via chromatography.

Bis[(5,5′-10,20-bis[4-(3-methoxy-3-methylbutoxy)phenyl]porphinato)zinc(II)]ethyne (12). Reagents: (5-bromo-10,20-bis[4-(3-methoxy-3-methylbutoxy)phenyl]porphinato)zinc(II) (53 mg, 0.068 mmol), (5-ethynyl-10,20-bis[4-(3-methoxy-3-methylbutoxy)phenyl]porphinato)zinc(II) (45 mg, 0.062 mmol), Pd₂(dba)₃ (9 mg, 0.0093 mmol), AsPh₃ (23 mg, 0.074 mmol), THF (10 mL), and triethylamine (2 mL). Reaction time, 3 h. Chromatographic purification: silica gel, 1:1 hexanes/THF, followed by SX-1 biobeads, THF. The dark green band was isolated, giving desired product **12** (0.083 g, 94% based on 45 mg of the porphyrinic starting material). ¹H NMR (250 MHz, 50:1 CDCl₃/pyridine-*d*₅): δ 10.45 (d, *J* = 4.53 Hz, 4H), 10.04 (s, 2H), 9.24 (d, *J* = 4.43 Hz, 4H), 9.15 (d, *J* = 4.43 Hz, 4H), 8.98 (d, *J* = 4.35 Hz, 4H), 8.16 (d, *J* = 8.43 Hz, 8H), 7.31 (d, *J* = 8.53 Hz, 8H), 4.38 (t, *J* = 7.26 Hz, 8H), 3.33 (s, 12H), 2.22 (t, *J* = 6.98 Hz, 8H), 1.37 (s, 24H). Visible (THF): 403 (5.08), 411 (5.08), 430 (5.00), 478 (5.46), 548 (4.21), 565 (4.18), 701 (4.69) nm. MS (MALDI-TOF) *m/z*: 1535 (calcd for C₉₀H₈₆N₈O₈Zn₂ 1535).

Bis[(2–5,10,15,20-tetraphenylporphinato)zinc(II)]ethyne (13). This compound was synthesized by methods reported previously.³¹

[(2–5,10,15,20-Tetraphenylporphinato)zinc(II)]–[5′–10′20′-bis[4-(3-methoxy-3-methylbutoxy)phenyl]porphinato]zinc(II)]ethyne (14). Reagents: (2-ethynyl-5,10,15,20-tetraphenylporphinato)zinc(II) (45 mg, 0.0641 mmol), (5-bromo-10,20-bis[4-(3-methoxy-3-methylbutoxy)phenyl]porphinato)zinc(II) (55 mg, 0.0705 mmol), Pd₂(dba)₃ (9 mg, 0.0096 mmol), AsPh₃ (24 mg, 0.0769 mmol), THF (10 mL), and triethylamine (2 mL). Reaction time, 26 h. Chromatographic purification: silica gel, 7:3 hexanes/THF. The green band was isolated, giving desired product **14** (51 mg, 57% based on 45 mg of the porphyrinic starting material). ¹H NMR (250 MHz, 50:1 CDCl₃/pyridine-*d*₅): δ 10.04 (s, 1H), 9.61 (d, *J* = 4.53 Hz, 2H), 9.50 (s, 1H), 9.24 (d, *J* = 4.43 Hz, 2H), 8.97 (d, *J* = 4.34 Hz, 2H), 8.91 (d, *J* = 4.43 Hz, 2H), 8.88 (s, 2H), 8.83 (s, 2H), 8.77 (d, *J* = 4.63 Hz, 1H), 8.72 (d, *J* = 4.53 Hz, 1H), 8.27 (m, 4H), 8.18 (m, 4H), 8.13 (d, *J* = 8.18 Hz, 4H), 7.67 (m, 9H), 7.27 (d, *J* = 8.18 Hz, 4H), 6.90 (t, *J* = 7.45 Hz, 2H), 5.67 (t, *J* = 7.48 Hz, 1H), 4.35 (t, *J* = 7.05 Hz, 4H), 3.31 (s, 6H), 2.19 (t, *J* = 7.00 Hz, 4H), 1.34 (s, 12H). Visible (THF): 433 (5.37), 447 (5.46), 566 (4.41), 613 (4.34) nm. MS (MALDI-TOF) *m/z*: 1452 (calcd for C₉₀H₇₀N₈O₄Zn₂ 1454).

[(2–5,10,15,20-Tetrakis(trifluoromethyl)porphinato)zinc(II)]–[(5′–10′20′-bis[4-(3-methoxy-3-methylbutoxy)phenyl]porphinato)zinc(II)]ethyne (15). Reagents: (5-ethynyl-10,20-bis[4-(3-methoxy-3-methylbutoxy)phenyl]porphinato)zinc(II) (40 mg, 0.055 mmol), [2-bromo-5,10,15,20-tetrakis(trifluoromethyl)porphinato]zinc(II) (48 mg, 0.066 mmol), Pd₂(dba)₃ (8 mg, 0.0083 mmol), AsPh₃ (20 mg, 0.066 mmol), THF (5 mL), and triethylamine (1 mL). Reaction time, 20 h. Chromatographic purification: silica gel, 3:1 hexanes/THF, followed by biobeads SX-1, THF. The dark green band was isolated, giving desired product **15** (65 mg, 86% based on 40 mg of the porphyrinic starting material). ¹H NMR (250 MHz, 50:1 CDCl₃/pyridine-*d*₅): δ

(23) Fletcher, J. T.; Therien, M. J. *J. Am. Chem. Soc.* **2000**, *122*, 12393–12394.

(24) Heck, R. F. *Acc. Chem. Res.* **1979**, *12*, 146–151.

(25) Kumada, M. *Pure Appl. Chem.* **1980**, *52*, 669–678.

(26) Negishi, E.-I.; Luo, F. T.; Frisbee, R.; Matsushita, H. *Heterocycles* **1982**, *18*, 117–122.

(27) Stille, J. K. *Angew. Chem., Int. Ed. Engl.* **1986**, *25*, 508–524.

(28) DiMugno, S. G.; Lin, V. S.-Y.; Therien, M. J. *J. Am. Chem. Soc.* **1993**, *115*, 2513–2515.

(29) DiMugno, S. G.; Lin, V. S.-Y.; Therien, M. J. *J. Org. Chem.* **1993**, *58*, 5983–5993.

(30) Lin, V. S.-Y.; DiMugno, S. G.; Therien, M. J. *Science* **1994**, *264*, 1105–1111.

(31) Lin, V. S.-Y.; Therien, M. J. *Chem. Eur. J.* **1995**, *1*, 645–651.

(32) Vollhardt, K. P. C. *Angew. Chem., Int. Ed. Engl.* **1984**, *23*, 539–644.

(33) Schore, N. E. *Chem. Rev.* **1988**, *88*, 1081–1119.

(34) Lautens, M.; Klute, W.; Tam, W. *Chem. Rev.* **1996**, *96*, 49–92.

(35) Tse, M. K.; Zhou, Z.; Mak, T. C. W.; Chan, K. S. *Tetrahedron* **2000**, *56*, 7779–7783.

(36) DiMugno, S. G.; Williams, R. A.; Therien, M. J. *J. Org. Chem.* **1994**, *59*, 6943–6948.

(37) Goll, J. G.; Moore, K. T.; Ghosh, A.; Therien, M. J. *J. Am. Chem. Soc.* **1996**, *118*, 8344–8354.

(38) Nishino, N.; Wagner, R. W.; Lindsey, J. S. *J. Org. Chem.* **1996**, *61*, 7534–7544.

(39) Wagner, R. W.; Johnson, T. E.; Li, F.; Lindsey, J. S. *J. Org. Chem.* **1995**, *60*, 5266–5273.

10.22 (q, $J = 2.70$ Hz, 1H), 10.21 (d, $J = 4.58$ Hz, 2H), 10.09 (s, 1H), 9.65 (m, 6H), 9.26 (d, $J = 4.53$ Hz, 2H), 9.15 (d, $J = 4.55$ Hz, 2H), 8.99 (d, $J = 4.43$ Hz, 2H), 8.15 (d, $J = 8.53$ Hz, 4H), 7.30 (d, $J = 8.63$ Hz, 4H), 4.39 (t, $J = 7.13$ Hz, 4H), 3.34 (s, 6H), 2.23 (t, $J = 7.14$ Hz, 4H), 1.38 (s, 12H). ^{19}F NMR (200 MHz, 50:1 $\text{CDCl}_3/\text{pyridine-}d_5$): δ -33.74 (s, 3F), -36.42 (s, 3F), -36.74 (s, 3F), -36.83 (s, 3F). Visible (THF): 432 (5.24), 565 (4.16), 612 (4.13), 700 (4.12) nm. MS (MALDI-TOF) m/z : 1423 (calcd for $\text{C}_{70}\text{H}_{50}\text{F}_{12}\text{N}_8\text{O}_4\text{Zn}$ 1423).

[(2'-5',10',15',20'-Tetrakis(trifluoromethyl)porphinato)zinc(II)]-(2'-5',10',15',20'-tetraphenylporphinato)zinc(II)ethyne (16). Reagents: (2-ethynyl-5,10,15,20-tetraphenylporphinato)zinc(II) (48 mg, 0.0684 mmol), [2-bromo-5,10,15,20-tetrakis(trifluoromethyl)porphinato]zinc(II) (50 mg, 0.0684 mmol), $\text{Pd}_2(\text{dba})_3$ (9 mg, 0.0103 mmol), AsPh_3 (25 mg, 0.0821 mmol), THF (10 mL), and triethylamine (2 mL). Reaction time, 17 h. Chromatographic purification: silica gel, 4:1 hexanes/THF. The purple-green band was isolated, giving desired product **16** (47 mg, 51% based on 48 mg of the porphyrinic starting material). ^1H NMR (250 MHz, 50:1 $\text{CDCl}_3/\text{pyridine-}d_5$): δ 9.65 (m, 7H), 9.38 (q, $J = 2.94$ Hz, 1H), 8.93 (d, $J = 4.79$ Hz, 1H), 8.86 (d, $J = 4.78$ Hz, 1H), 8.83 (s, 2H), 8.80 (d, $J = 4.84$ Hz, 1H), 8.75 (d, $J = 4.64$ Hz, 1H), 8.36 (m, 4H), 8.19 (m, 4H), 7.85 (m, 3H), 7.73 (m, 9H). ^{19}F NMR (200 MHz, 50:1 $\text{CDCl}_3/\text{pyridine-}d_5$): δ -34.24 (s, 3F), -36.51 (s, 3F), -36.83 (s, 3F), -37.10 (s, 3F). Visible (THF): 431 (5.39), 565 (4.37), 645 (4.47) nm. MS (MALDI-TOF) m/z : 1343 (calcd for $\text{C}_{70}\text{H}_{34}\text{F}_{12}\text{N}_8\text{Zn}$ 1342).

Bis[(2-5,15-(trifluoromethyl)-10,20-diphenylporphinato)zinc(II)]ethyne (17). Reagents: [2-bromo-5,15-bis(trifluoromethyl)-10,20-diphenylporphinato]zinc(II) (42 mg, 0.0612 mmol), [2-ethynyl-5,15-bis(trifluoromethyl)-10,20-diphenylporphinato]zinc(II) (49 mg, 0.0661 mmol), Pd_2dba_3 (8 mg, 0.0092 mmol), AsPh_3 (15 mg, 0.0735 mmol), THF (5 mL), and triethylamine (1 mL). Reaction time, 19 h. Chromatographic purification: silica gel, 1:1 hexanes/toluene. The final green band was isolated, giving desired product **17** (37 mg, 45% based on 42 mg of the (bromoporphinato)zinc(II) starting material). ^1H NMR (250 MHz, 50:1 $\text{CDCl}_3/\text{pyridine-}d_5$): δ 9.70–9.40 (m, 6H), 8.90–8.70 (m, 8H), 8.30–7.90 (m, 8H), 7.90–7.40 (m, 12H). ^{19}F NMR (200 MHz, 50:1 $\text{CDCl}_3/\text{pyridine-}d_5$): δ -32.45 (s, 3F), -35.74 (s, 3F). Visible (THF): 427 (5.21), 573 (4.17), 628 (sh) (4.54), 646 (4.66) nm. MS (MALDI-TOF) m/z : 1342 (calcd for $\text{C}_{70}\text{H}_{34}\text{F}_{12}\text{N}_8\text{Zn}$ 1342).

Bis[(2-5,10,15,20-tetrakis(trifluoromethyl)porphinato)zinc(II)]ethyne (18). Reagents: [2-bromo-5,10,15,20-tetrakis(trifluoromethyl)porphinato]zinc(II) (61 mg, 0.0840 mmol), [2-ethynyl-5,10,15,20-tetrakis(trifluoromethyl)porphinato]zinc(II) (48 mg, 0.0700 mmol), Pd_2dba_3 (10 mg, 0.0105 mmol), AsPh_3 (26 mg, 0.0840 mmol), THF (10 mL), and triethylamine (2 mL). Reaction time, 17 h. Chromatographic purification: silica gel, 1:1 hexanes/toluene. The final green band was isolated, giving desired product **18** (67 mg, 73% based on 48 mg of the porphyrinic starting material). ^1H NMR (50:1 $\text{CDCl}_3/\text{pyridine-}d_5$): δ 10.09 (q, $J = 2.78$ Hz, 2H), 9.78 (m, 2H), 9.66 (m, 10H). ^{19}F NMR (200 MHz, 50:1 $\text{CDCl}_3/\text{pyridine-}d_5$): δ -33.71 (s, 3F), -36.51 (s, 3F), -36.80 (s, 3F), -36.95 (s, 3F). Visible (THF): 425 (5.20), 572 (4.20), 620 (sh) (4.31), 655 (4.68) nm. MS (MALDI-TOF) m/z : 1311 (calcd for $\text{C}_{50}\text{H}_{14}\text{F}_{24}\text{N}_8\text{Zn}$ 1310).

General Procedure for the Preparation of (Phenylethynylporphinato)zinc(II) Complexes.^{40,41} A 50-mL Schlenk tube was charged with ethynylbenzene (5–20 equiv), a *meso*- or β -bromoporphyrin (1 equiv), $\text{Pd}_2(\text{dba})_3$ (0.15 equiv), and AsPh_3 (1.2 equiv). These reagents were dissolved in 5:1 THF/TEA and stirred for 14–20 h at 40 °C. Following evaporation of the solvent, the residue was purified via chromatography.

(10,20-Bis[4-(3-methoxy-3-methylbutoxy)phenyl]-5-(phenylethynyl)porphinato)zinc(II) (19). Reagents: (5-bromo-10,20-bis[4-(3-

methoxy-3-methylbutoxy)phenyl]porphinato)zinc(II) (0.300 g, 0.384 mmol), ethynylbenzene (0.21 mL, 1.92 mmol), $\text{Pd}_2(\text{dba})_3$ (0.053 g, 0.058 mmol), AsPh_3 (0.141 g, 0.461 mmol), THF (15 mL), and triethylamine (3 mL). Reaction time, 14 h. Chromatographic purification: silica gel, 3:1 hexanes/THF. The dark green band was isolated, giving desired product **19** (0.270 g, 88% based on 300 mg of the (bromoporphinato)zinc(II) starting material). ^1H NMR (250 MHz, 50:1 $\text{CDCl}_3/\text{pyridine-}d_5$): δ 10.04 (s, 1H), 9.77 (d, $J = 4.45$ Hz, 2H), 9.22 (d, $J = 4.43$ Hz, 2H), 8.98 (d, $J = 4.68$ Hz, 2H), 8.93 (d, $J = 4.48$ Hz, 2H), 8.07 (d, $J = 8.40$ Hz, 4H), 8.00 (m, 2H), 7.49 (m, 2H), 7.43 (m, 1H), 7.26 (d, $J = 8.40$ Hz, 4H), 4.36 (t, $J = 7.16$ Hz, 4H), 3.32 (s, 6H), 2.20 (t, $J = 7.14$ Hz, 4H), 1.36 (s, 12H). Visible (THF): 435 (5.57), 529 (3.55), 567 (4.19), 615 (4.26) nm. MS (MALDI-TOF) m/z : 856 (calcd for $\text{C}_{52}\text{H}_{49}\text{N}_4\text{O}_4\text{Zn}$ 856).

[5,10,15,20-Tetraphenyl-2-(phenylethynyl)porphinato]zinc(II) (20). Reagents: (2-ethynyl-5,10,15,20-tetraphenylporphinato)zinc(II) (68 mg, 0.097 mmol), iodobenzene (0.11 mL, 0.97 mmol), $\text{Pd}_2(\text{dba})_3$ (13 mg, 0.015 mmol), AsPh_3 (0.036 g, 0.116 mmol), THF (5 mL), and triethylamine (1 mL). Reaction time, 20 h. Chromatographic purification: silica gel, 4:1 hexanes/THF. The purple-green band was isolated, giving desired product **20** (59 mg, 78% based on 68 mg of the porphyrinic starting material). ^1H NMR (250 MHz, 50:1 $\text{CDCl}_3/\text{pyridine-}d_5$): δ 9.14 (s, 1H), 8.81 (s, 2H), 8.80 (s, 2H), 8.76 (d, $J = 4.67$ Hz, 1H), 8.67 (d, $J = 4.68$ Hz, 1H), 8.15 (m, 8H), 7.67 (m, 14H), 7.35 (m, 3H). Visible (THF): 432, 524, 564, 600 nm. MS (MALDI-TOF) m/z : 776 (calcd for $\text{C}_{52}\text{H}_{32}\text{N}_4\text{Zn}$ 776).

[5,15-Bis(trifluoromethyl)-10,20-diphenyl-2-(phenylethynyl)porphinato]zinc(II) (21). Reagents: [2-bromo-5,15-bis(trifluoromethyl)-10,20-diphenylporphinato]zinc(II) (23 mg, 0.031 mmol), ethynylbenzene (34 μL , 0.31 mmol), Pd_2dba_3 (4 mg, 0.0047 mmol), AsPh_3 (11 mg, 0.0372 mmol), THF (5 mL), and triethylamine (1 mL). Reaction time, 17 h. Chromatographic purification: silica gel, 1:1 hexanes/toluene. The green band was isolated, giving desired product **21** (18 mg, 76% based on 23 mg of the (bromoporphinato)zinc(II) starting material). ^1H NMR (250 MHz, 50:1 $\text{CDCl}_3/\text{pyridine-}d_5$): δ 9.53 (m, 3H), 8.86 (s, 1H), 8.80 (d, $J = 4.98$ Hz, 1H), 8.77 (d, $J = 4.71$ Hz, 1H), 8.75 (d, $J = 4.082$ Hz, 1H), 8.07 (m, 4H), 7.78 (m, 2H), 7.70 (m, 6H), 7.40 (m, 3H). ^{19}F NMR (200 MHz, 50:1 $\text{CDCl}_3/\text{pyridine-}d_5$): δ -32.39 (s, 3F), -35.77 (s, 3F). Visible (THF): 430 (5.13), 571 (3.89), 615 (4.30) nm. MS (MALDI-TOF) m/z : 760 (calcd for $\text{C}_{42}\text{H}_{22}\text{F}_6\text{N}_4\text{Zn}$ 760).

[5,10,15,20-Tetrakis(trifluoromethyl)-2-(phenylethynyl)porphinato]zinc(II) (22). Reagents: [2-bromo-5,10,15,20-tetrakis(trifluoromethyl)porphinato]zinc(II) (45 mg, 0.0621 mmol), ethynylbenzene (37 mL, 0.336 mmol), Pd_2dba_3 (9 mg, 0.0101 mmol), AsPh_3 (25 mg, 0.0806 mmol), THF (5 mL), and triethylamine (1 mL). Reaction time, 20 h. Chromatographic purification: silica gel, 1:1 hexanes/toluene. The green band was isolated, giving desired product **22** (41 mg, 89% based on 45 mg of the (bromoporphinato)zinc(II) starting material). ^1H NMR (50:1 $\text{CDCl}_3/\text{pyridine-}d_5$): δ 9.69 (q, $J = 2.86$ Hz, 1H), 9.58 (m, 5H), 7.85 (m, 2H), 7.46 (m, 2H), 7.10 (m, 1H). ^{19}F NMR (200 MHz, 50:1 $\text{CDCl}_3/\text{pyridine-}d_5$): δ -33.79 (s, 3F), -36.55 (s, 3F), -36.84 (s, 3F), -37.12 (s, 3F); visible (THF) 424 (5.03), 574 (3.98), 624 (4.36) nm. MS (MALDI-TOF) m/z : 743 (calc for $\text{C}_{32}\text{H}_{12}\text{F}_{12}\text{N}_4\text{Zn}$ 744).

Standard Procedure for the Syntheses of Cofacial Bis[(porphinato)zinc(II)] Compounds.^{23,42} A 50-mL Schlenk tube was charged with an ethyne-bridged bis[(porphinato)zinc(II)] compound (1 equiv) and $\text{Co}_2(\text{CO})_8$ (1 equiv). These reagents were dissolved in 5:1 toluene/dioxane and heated to 100 °C; dropwise addition of 5 mL of a toluene solution containing 1,6-heptadiyne (20 equiv) and $\text{Co}_2(\text{CO})_8$ (1 equiv) over a 17-h period followed. After the addition was complete, the solution was evaporated to dryness and the residue purified by chromatography.

5,6-Bis[(5',5''-10',20'-bis[4-(3-methoxy-3-methylbutoxy)phenyl]porphinato)zinc(II)]indane (1). Reagents: **12** (50 mg, 35 μmol), Co_2 -

(42) Fletcher, J. T.; Therien, M. J. *Inorg. Chem.* **2002**, *41*, 331-341.

(40) LeCours, S. M.; Guan, H.-W.; DiMaggio, S. G.; Wang, C. H.; Therien, M. J. *J. Am. Chem. Soc.* **1996**, *118*, 1497–1503.

(41) LeCours, S. M.; DiMaggio, S. G.; Therien, M. J. *J. Am. Chem. Soc.* **1996**, *118*, 11854–11864.

(CO)₈ (12 mg, 35 μmol), dioxane, (2.5 mL), and toluene (10 mL). Added dropwise: 1,6-heptadiyne (40 μL, 350 μmol) and Co₂(CO)₈ (12 mg, 35 μmol). Chromatographic purification: silica gel, 3:2 hexanes/THF. The red band was isolated, giving desired product **1** (50 mg, 94% based on 50 mg of starting material **12**). ¹H NMR (250 MHz, pyridine-*d*₅): δ 10.31 (d, *J* = 4.65 Hz, 4H), 10.11 (s, 2H), 9.29 (d, *J* = 4.50 Hz, 4H), 9.13 (d, *J* = 4.68 Hz, 4H), 8.95 (d, *J* = 4.48 Hz, 4H), 8.64 (s, 2H), 8.02 (d, *J* = 8.28 Hz, 4H), 7.66 (d, *J* = 8.25 Hz, 4H), 7.32 (d, *J* = 8.33 Hz, 4H), 7.25 (d, *J* = 8.45 Hz, 4H), 4.43 (t, *J* = 7.06 Hz, 8H), 3.41 (t, *J* = 6.88 Hz, 4H), 3.30 (s, 12H), 2.40 (m, 2H), 2.26 (t, *J* = 6.98 Hz, 8H), 1.36 (s, 24H). Visible (THF): 411 (5.54), 434 (4.74), 558 (4.32), 589 (3.72), 599 (3.71) nm. MS (MALDI-TOF) *m/z*: 1627 (calcd for C₉₇H₉₄N₈O₈Zn₂ 1627).

5,6-Bis[(2'-5',10',15',20'-tetraphenylporphinato)zinc(II)]indane (2). Reagents: **13** (25 mg, 18.1 μmol), Co₂(CO)₈ (6 mg, 18.1 μmol), dioxane (1 mL), and toluene (4 mL). Added dropwise: 1,6-heptadiyne (41 μL, 362 μmol) and Co₂(CO)₈ (6 mg, 18.1 μmol). Chromatographic purification: silica gel, 1:1 hexanes/toluene. The purple band was isolated, giving desired product **2** (12 mg, 45% based on 25 mg of starting material **13**). ¹H NMR (250 MHz, 50:1 CDCl₃/pyridine-*d*₅): δ 8.46–8.92 (m, 14H), 6.80–8.42 (m, 42 H), 2.96 (d, *J* = 7.2 Hz, 2H), 2.83 (t, *J* = 7.2 Hz, 2H), 2.10 (m, 2H). Visible (THF): 424 (5.44), 561 (4.34), 599 (3.92) nm. MS (MALDI-TOF) *m/z*: 1468 (calcd for C₉₇H₆₂N₈Zn₂ 1466).

5-[(2'-5',10',15',20'-Tetraphenylporphinato)zinc(II)]-6-[(5''-10'',20''-bis[4-(3-methoxy-3-methylbutoxy)phenyl]porphinato)zinc(II)]indane (3). Reagents: **14** (25 mg, 17.8 μmol), Co₂(CO)₈ (6 mg, 17.9 μmol), dioxane (1 mL), and toluene (5 mL). Added dropwise: 1,6-heptadiyne (41 μL, 357 μmol) and Co₂(CO)₈ (6 mg, 17.9 μmol). Chromatographic purification: silica gel, 4:1 hexanes/THF. The first green band was isolated, giving desired product **3** (18 mg, 67% based on 25 mg of starting material **14**). ¹H NMR (250 MHz, 50:1 CDCl₃/pyridine-*d*₅): δ 9.86 (s, 1H), 9.52 (d, *J* = 4.61 Hz, 1H), 9.23 (d, *J* = 4.51 Hz, 1H), 9.06 (d, *J* = 4.37 Hz, 1H), 8.97 (d, *J* = 4.38 Hz, 1H), 8.96 (d, *J* = 4.25 Hz, 1H), 8.92 (d, *J* = 4.57 Hz, 1H), 8.75 (m, 2H), 8.61 (m, 6H), 8.49 (d, *J* = 4.70 Hz, 1H), 8.32 (d, *J* = 4.68 Hz, 1H), 8.09 (m, 1H), 7.98 (m, 3H), 7.86 (m, 3H), 7.58 (m, 16H), 7.25 (m, 2H), 7.14 (m, 2H), 7.03 (m, 1H), 6.87 (m, 1H), 6.36 (m, 1H), 4.54 (m, 1H), 4.46 (t, *J* = 7.18 Hz, 2H), 4.17 (t, *J* = 7.15 Hz, 2H), 3.37 (s, 3H), 3.23 (s, 3H), 3.04 (t, *J* = 6.80 Hz, 4H), 2.28 (t, *J* = 7.09 Hz, 4H), 2.07 (t, *J* = 7.12 Hz, 2H), 1.42 (s, 6H), 1.26 (s, 6H). Visible (THF): 418 (5.45), 438 (5.09), 555 (4.31), 595 (3.76) nm. MS (MALDI-TOF) *m/z*: 1546 (calcd for C₉₇H₇₈N₈O₄Zn₂ 1546). The final green band was also collected, which corresponded to pure starting material **14** (8 mg, 32%).

5-[(2'-5',10',15',20'-Tetrakis(trifluoromethyl)porphinato)zinc(II)]-6-[(5''-10'',20''-bis[4-(3-methoxy-3-methylbutoxy)phenyl]porphinato)zinc(II)]indane (4). Reagents: **15** (25 mg, 18.2 μmol), Co₂(CO)₈ (6 mg, 18.2 μmol), dioxane (1 mL), and toluene (5 mL). Added dropwise: 1,6-heptadiyne (21 μL, 182 μmol) and Co₂(CO)₈ (6 mg, 18.2 μmol). Chromatographic purification: silica gel, 4:1 hexanes/THF. The first green band was isolated, giving desired product **4** (11 mg, 41% based on 25 mg of starting material **15**). ¹H NMR (250 MHz, 50:1 CDCl₃/pyridine-*d*₅): δ 9.95 (s, 1H), 9.52 (s, 2H), 9.41 (s, 3H), 9.27 (d, *J* = 4.53 Hz, 1H), 9.19 (m, 1H), 9.16 (d, *J* = 4.73 Hz, 1H), 9.10 (d, *J* = 4.43 Hz, 1H), 9.05 (d, *J* = 4.45 Hz, 1H), 9.04 (d, *J* = 4.48 Hz, 1H), 8.92 (m, 1H), 8.81 (d, *J* = 4.55 Hz, 1H), 8.79 (m, 1H), 8.76 (d, *J* = 4.43 Hz, 1H), 8.42 (s, 1H), 8.38 (dd, *J*₁ = 8.27 Hz, *J*₂ = 2.05 Hz, 1H), 8.07 (dd, *J*₁ = 8.27 Hz, *J*₂ = 1.96 Hz, 1H), 7.87 (dd, *J*₁ = 8.27 Hz, *J*₂ = 2.00 Hz, 1H), 7.81 (dd, *J*₁ = 8.53 Hz, *J*₂ = 2.00 Hz, 1H), 7.43 (dd, *J*₁ = 8.49 Hz, *J*₂ = 2.20 Hz, 1H), 7.28 (dd, *J*₁ = 11.41 Hz, *J*₂ = 3.16 Hz, 1H), 7.15 (dd, *J*₁ = 10.8 Hz, *J*₂ = 2.45 Hz, 1H), 7.09 (dd, *J*₁ = 10.8 Hz, *J*₂ = 2.45 Hz, 1H), 4.41 (t, *J* = 7.13 Hz, 2H), 4.28 (t, *J* = 7.18 Hz, 2H), 3.45 (m, 4H), 3.33 (s, 3H), 3.27 (s, 3H), 2.48 (m, 2H), 2.24 (t, *J* = 7.15 Hz, 2H), 2.14 (t, *J* = 7.15 Hz, 2H), 1.38 (s, 6H), 1.31 (s, 6H). ¹⁹F NMR (200 MHz, 50:1 CDCl₃/pyridine-*d*₅): δ -31.50 (s, 3F), -36.51 (s, 3F), -36.72 (s, 3F), -38.36 (s, 3F).

Visible (THF): 418 (5.43), 555 (4.26), 612 (4.22) nm. MS (MALDI-TOF) *m/z*: 1514 (calcd for C₇₇H₅₈F₁₂N₈O₄Zn₂ 1514). The final green-brown band was also isolated, giving pure recovered starting material **15** (14 mg, 55%).

5-(2'-5',10',15',20'-[Tetrakis(trifluoromethyl)porphinato]zinc(II)]-6-[(2''-5'',10'',15'',20''-tetraphenylporphinato)zinc(II)]indane (5). Reagents: **16** (35 mg, 26 μmol), Co₂(CO)₈ (9 mg, 26 μmol), dioxane (1 mL), and toluene (5 mL). Added dropwise: 1,6-heptadiyne (30 μL, 260 μmol) and Co₂(CO)₈ (9 mg, 26 μmol). Chromatographic purification: silica gel, 4:1 hexanes/THF. The first green band was isolated, giving desired product **5** (13 mg, 35% based on 35 mg of starting material **16**). ¹H NMR (250 MHz, 50:1 CDCl₃/pyridine-*d*₅): δ 9.74 (m, 1H), 9.63 (m, 1H), 9.57 (m, 2H), 9.37 (m, 1H), 9.13 (m, 1H), 9.04 (m, 1H), 8.93 (s, 1H), 8.90 (d, *J* = 4.71 Hz, 1H), 8.88 (d, *J* = 4.68 Hz, 1H), 8.86 (d, *J* = 4.66 Hz, 1H), 8.82 (d, *J* = 4.60 Hz, 1H), 8.74 (d, *J* = 4.60 Hz, 1H), 8.65 (d, *J* = 4.66 Hz, 1H), 8.44 (m, 1H), 8.30 (m, 1H), 8.23 (m, 4H), 8.16 (m, 4H), 7.70 (m, 8H), 7.10 (m, 2H), 6.64 (m, 2H), 2.83 (m, 4H), 2.08 (m, 2H). ¹⁹F NMR (200 MHz, 50:1 CDCl₃/pyridine-*d*₅): δ -32.79 (s, 3F), -36.07 (s, 3F), -36.36 (s, 3F), -38.19 (s, 3F). Visible (THF): 426 (5.36), 562 (4.83), 612 (4.22) nm. MS (MALDI-TOF) *m/z*: 1436 (calcd for C₇₇H₄₂F₁₂N₈Zn₂ 1434). A slower brown-green band, following the product band, was also isolated, giving pure recovered starting material **16** (21 mg, 60%).

5,6-Bis[(2'-5',15'-[trifluoromethyl]-10',20'-diphenylporphinato)zinc(II)]indane (6). Reagents: **17** (22 mg, 16.7 μmol), Co₂(CO)₈ (6.5 mg, 18.6 μmol), dioxane (1 mL), and toluene (4 mL). Added dropwise: 1,6-heptadiyne (25 μL, 186 μmol) and Co₂(CO)₈ (6.5 mg, 18.6 μmol). Chromatographic purification: silica gel, 100:100:1 hexanes/toluene/THF. The green band was isolated, giving desired product **6** (12 mg, 45% based on 22 mg of starting material **17**). ¹H NMR (250 MHz, 50:1 CDCl₃/pyridine-*d*₅): δ 9.67 (m, 2H), 9.49 (m, 2H), 9.42 (m, 2H), 8.95–8.60 (m, 8H), 8.42 (s, 2H), 8.10–7.40 (m, 18H), 6.48 (m, 2H), 3.05 (m, 4H), 2.15 (m, 2H). ¹⁹F NMR (200 MHz, 50:1 CDCl₃/pyridine-*d*₅): δ -31.00 (s, 3F), -35.68 (s, 3F). Visible (THF): 419 (5.30), 564 (4.12), 610 (4.41) nm. MS (MALDI-TOF) *m/z*: 1434 (calcd for C₇₇H₄₂F₁₂N₈Zn₂ 1434).

5,6-Bis[(2'-5',10',15',20'-tetrakis(trifluoromethyl)porphinato)zinc(II)]indane (7). Reagents: **18** (16 mg, 12.2 μmol), dioxane (1 mL), and toluene (4 mL). Added dropwise: 1,6-heptadiyne (28 μL, 243 μmol) and Co₂(CO)₈ (8 mg, 24.3 μmol). Chromatographic purification: silica gel, 1:1 hexanes/toluene. The green band was isolated, giving desired product **7** (6 mg, 29% based on 16 mg of starting material **18**). ¹H NMR (250 MHz, 50:1 CDCl₃/pyridine-*d*₅): δ 9.65 (m, 2H), 9.53 (m, 4H), 9.12 (dq, *J*₁ = 2.22 Hz, *J*₂ = 3.01 Hz, 2H), 8.67 (dq, *J*₁ = 2.60 Hz, *J*₂ = 2.63 Hz, 2H), 8.48 (m, 2H), 8.35 (s, 2H), 8.18 (dq, *J*₁ = 2.50 Hz, *J*₂ = 2.67 Hz, 2H), 3.45 (m, 4H), 2.51 (m, 2H). ¹⁹F NMR (200 MHz, 50:1 CDCl₃/pyridine-*d*₅): δ -34.29 (s, 3F), -36.23 (s, 3F), -36.45 (s, 3F), -37.16 (s, 3F). Visible (THF): 399 (5.18), 570 (3.94), 608 (4.23) nm. MS (MALDI-TOF) *m/z*: 1400 (calcd for C₅₇H₂₂F₂₄N₈-Zn₂ 1402). The final green band was also isolated, giving pure recovered starting material **18** (14 mg, 63%).

Standard Procedure for Metal-Templated Cycloaddition Reactions Involving (Phenylethynylporphinato)zinc(II) Substrates.²³ A 50-mL Schlenk tube was charged with a (phenylethynylporphinato)zinc(II) compound (1 equiv) and Co₂(CO)₈ (1 equiv). These reagents were dissolved in 5:1 toluene/dioxane and heated to 100 °C; dropwise addition of 5 mL of a toluene solution containing 1,6-heptadiyne (10 eq) over a 90-min period followed. After the addition was complete, the solution was evaporated to dryness and the residue purified by chromatography.

5-Phenyl-6-[(5'-10',20'-bis[4-(3-methoxy-3-methylbutoxy)phenyl]porphinato)zinc(II)]indane (8). Reagents: **19** (40 mg, 46.6 μmol), Co₂(CO)₈ (16 mg, 46.6 μmol), dioxane (1 mL), and toluene (4 mL). Added dropwise: 1,6-heptadiyne (53 μL, 466 μmol). Chromatographic purification: silica gel, 4:1 hexanes/THF. The purple band was isolated, giving desired product **8** (44 mg, 99% based on 40 mg of starting

material **19**). ^1H NMR (250 MHz, 50:1 $\text{CDCl}_3/\text{pyridine-}d_5$): δ 10.11 (s, 1H), 9.21 (d, $J = 4.48$ Hz, 2H), 8.93 (d, $J = 4.43$ Hz, 2H), 8.87 (d, $J = 4.60$ Hz, 2H), 8.81 (d, $J = 4.55$ Hz, 2H), 8.03 (m, 4H), 7.81 (s, 1H), 7.57 (s, 1H), 7.20 (m, 4H), 7.08 (m, 2H), 6.24 (m, 3H), 4.32 (t, $J = 7.37$ Hz, 4H), 3.30 (s, 6H), 3.24 (t, $J = 7.34$ Hz, 2H), 3.07 (t, $J = 7.32$ Hz, 2H), 2.30 (m, 2H), 2.18 (t, $J = 7.14$ Hz, 4H), 1.34 (s, 12H). Visible (THF): 422 (5.56), 552 (4.21), 592 (3.57) nm. MS (MALDI-TOF) m/z : 948 (calcd for $\text{C}_{59}\text{H}_{56}\text{N}_4\text{O}_4\text{Zn}$ 948).

5-Phenyl-6-[(2'-5',10',15',20'-tetraphenylporphinato)zinc(II)]indane (9). Reagents: **20** (59 mg, 75.8 μmol), $\text{Co}_2(\text{CO})_8$ (26 mg, 75.8 μmol), dioxane (2 mL), and toluene (8 mL). Added dropwise: 1,6-heptadiyne (86 μL , 758 μmol). Chromatographic purification: silica gel, 4:1 hexanes/THF. The purple band was isolated, giving desired product **9** (64 mg, 97% based on 59 mg of starting material **20**). ^1H NMR (250 MHz, 50:1 $\text{CDCl}_3/\text{pyridine-}d_5$): δ 8.83 (s, 2H), 8.81 (s, 1H), 8.80 (s, 1H), 8.72 (d, $J = 4.71$ Hz, 1H), 8.58 (d, $J = 4.69$ Hz, 1H), 8.45 (s, 1H), 8.15 (m, 6H), 7.90–7.10 (m, 18H), 7.06 (m, 2H), 6.75 (m, 1H), 6.65 (m, 2H), 2.93 (t, $J = 7.25$ Hz, 2H), 2.78 (t, $J = 7.33$ Hz, 2H), 2.10 (m, 2H). Visible (THF): 427 (5.55), 558 (4.16), 597 (3.92) nm. MS (MALDI-TOF) m/z : 868 (calcd for $\text{C}_{59}\text{H}_{40}\text{N}_4\text{Zn}$ 868).

5-Phenyl-6-[(2'-5',15'-bis(trifluoromethyl)-10',20'-diphenylporphinato)zinc(II)]indane (10). Reagents: **21** (30 mg, 39.4 μmol), $\text{Co}_2(\text{CO})_8$ (13 mg, 26.8 μmol), dioxane (1 mL), and toluene (5 mL). Added dropwise: 1,6-heptadiyne (45 μL , 394 μmol). Chromatographic purification: silica gel, 1:1 hexanes/toluene. The green band was isolated, giving desired product **10** (26 mg, 77% based on 30 mg of starting material **21**). ^1H NMR (250 MHz, 50:1 $\text{CDCl}_3/\text{pyridine-}d_5$): δ 9.54 (m, 3H), 8.85 (d, $J = 4.83$ Hz, 1H), 8.83 (d, $J = 4.79$ Hz, 1H), 8.79 (d, $J = 4.98$ Hz, 1H), 8.39 (m, 1H), 8.02 (s, 1H), 7.88–7.42 (m, 13H), 7.10 (m, 3H), 3.12 (m, 2H), 2.98 (m, 2H), 2.20 (m, 2H). ^{19}F NMR (200 MHz, 50:1 $\text{CDCl}_3/\text{pyridine-}d_5$): δ -31.22 (s, 3F), -35.65 (s, 3F). Visible (THF): 424 (5.24), 566 (3.94), 608 (4.24) nm. MS (MALDI-TOF) m/z : 853 (calcd for $\text{C}_{49}\text{H}_{30}\text{F}_6\text{N}_4\text{Zn}$ 852).

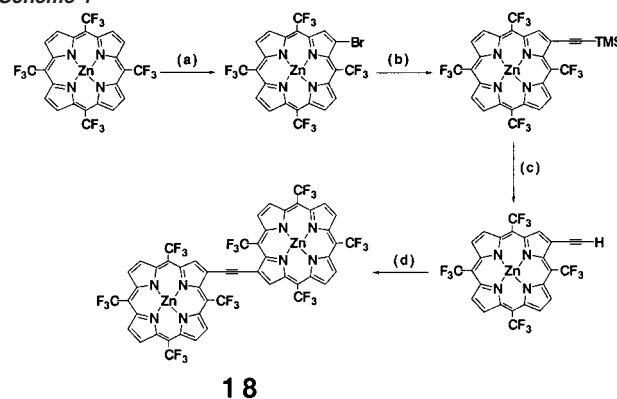
5-Phenyl-6-[(2'-5',10',15',20'-tetrakis(trifluoromethyl)porphinato)zinc(II)]indane (11). Reagents: **22** (20 mg, 26.8 μmol), $\text{Co}_2(\text{CO})_8$ (9 mg, 26.8 μmol), dioxane (1 mL), and toluene (4 mL). Added dropwise: 1,6-heptadiyne (31 μL , 268 μmol). Chromatographic purification: silica gel, 1:1 hexanes/toluene. The green band was isolated, giving desired product **11** (20 mg, 89% based on 20 mg of starting material **22**). ^1H NMR (250 MHz, 50:1 $\text{CDCl}_3/\text{pyridine-}d_5$): δ 9.61 (m, 5H), 9.40 (dq, $J_1 = 2.51$ Hz, $J_2 = 2.70$ Hz, 1H), 9.01 (q, $J = 3.07$ Hz, 1H), 7.72 (s, 1H), 7.51 (s, 1H), 7.07 (m, 2H), 6.52 (m, 3H), 3.15 (m, 4H), 2.27 (m, 2H). ^{19}F NMR (200 MHz, 50:1 $\text{CDCl}_3/\text{pyridine-}d_5$): δ -33.18 (s, 3F), -36.15 (s, 3F), -36.57 (s, 3F), -37.21 (s, 3F). Visible (THF): 420 (5.10), 570 (3.96), 612 (4.22) nm. MS (MALDI-TOF) m/z : 837 (calcd for $\text{C}_{39}\text{H}_{20}\text{F}_{12}\text{N}_4\text{Zn}$ 836).

Results and Discussion

Synthesis. Recently, we reported a synthetic route that utilizes cobalt-mediated cycloaddition of ethyne-elaborated porphyrin substrates to give 5,6-indanyl-bridged cofacial porphyrin structures.²³ In this study, we exploit the modular nature of this synthetic method, varying the electronic properties of the porphyrin units and the topological connectivity between these species, to establish the extent to which the overall electronic properties of cofacial (porphinato)metal complexes can be regulated.

A series of monomeric aryl- and perfluoroalkyl-functionalized (porphinato)zinc(II) units were employed as building blocks in these syntheses. The electronic properties of these two broad classes of (porphinato)zinc(II) compounds vary markedly; note, for example, that [5,10,15,20-tetrakis(perfluoroalkyl)porphinato]zinc(II) complexes possess HOMO and LUMO levels that are

Scheme 1^a



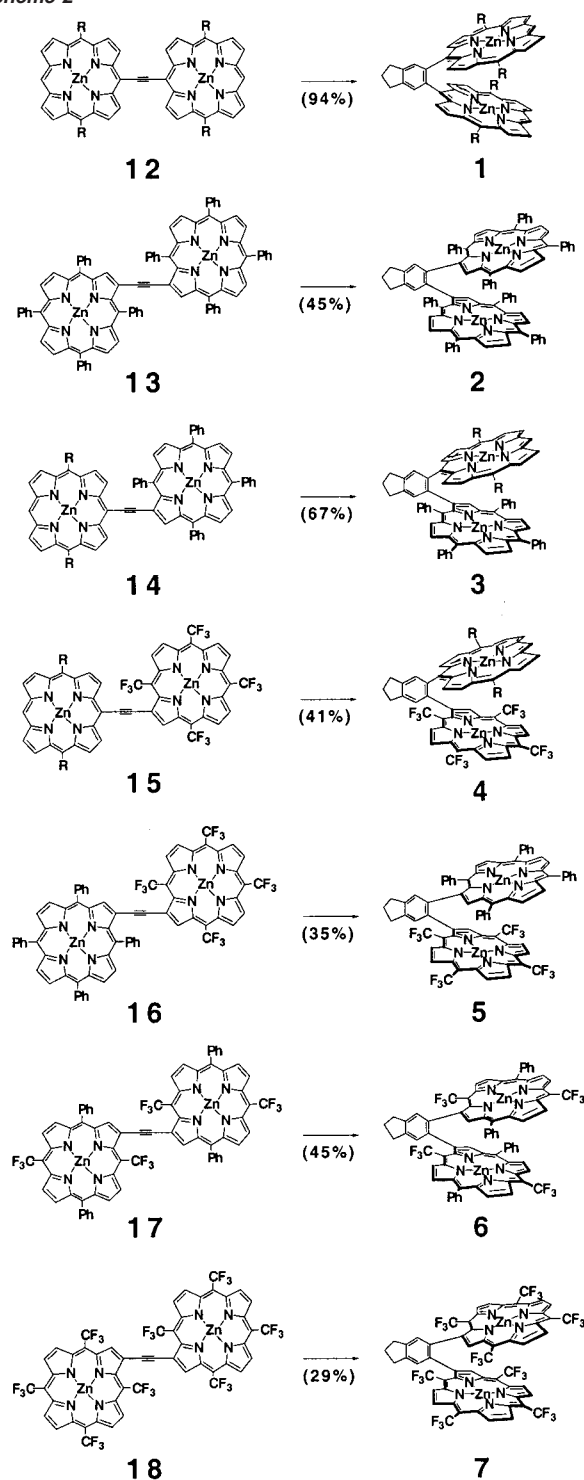
18

^a Reagents and conditions: (a) *N*-bromosuccinimide (1.1 equiv), methanol, reflux, 1.5 h (42%); (b) trimethylsilylacetylene (10 equiv), $\text{Pd}(\text{PPh}_3)_3\text{Cl}_2$ (10 mol %), CuI (10 mol %), THF/TEA 5:2, 40 °C, 17 h (75%); (c) (i) TBAF (2 equiv), THF, 10 min, (ii) NaHCO_3 (aq) (96%); (d) **1** (1.2 equiv), $\text{Pd}_2(\text{dba})_3$ (15 mol %), AsPh_3 (1.2 equiv), THF/TEA 5:1, 40 °C, 17 h (73%).

stabilized uniformly by nearly 700 mV^{36,37} relative to their corresponding (5,10,15,20-tetraphenylporphinato)zinc(II) benchmarks.

Macrocycle-to-macrocycle ethyne-bridged bis[(porphinato)metal] compounds^{30,31} serve as key precursors to cofacial porphyrin compounds synthesized via metal-templated cycloaddition reactions. The synthesis of the extremely electron-poor ethyne-linked dimeric (porphinato)zinc(II) species, bis[[(2,2'-5,10,15,20-trifluoromethyl)porphinato]zinc(II)]ethyne (**18**), is depicted in Scheme 1. [(5,10,15,20-Trifluoromethyl)porphinato]zinc(II)³⁷ can be readily brominated with *N*-bromosuccinimide,^{28,29,35,43,44} producing [(2-bromo-5,10,15,20-trifluoromethyl)porphinato]zinc(II); palladium-catalyzed cross-coupling with trimethylsilylacetylene gives the ethyne-elaborated macrocycle [5,10,15,20-(trifluoromethyl)-2-(trimethylsilylethynyl)porphinato]zinc(II). Deprotection with TBAF yields [(2-ethynyl-5,10,15,20-trifluoromethyl)porphinato]zinc(II), which can be cross-coupled with [(2-bromo-5,10,15,20-trifluoromethyl)porphinato]zinc(II) to afford **18**. Compound **18** serves as the first example of an electron-deficient ethyne-bridged bis[(porphinato)metal] species; notably these reactions demonstrate that perfluoroalkyl-substituted porphyrin macrocycles can be both suitably derivatized and coupled in yields comparable to that established previously for their electron-rich counterparts.^{28–31,40,41}

As such, ethyne-bridged precursor compounds bis[5,5'-10,20-bis[4-(3-methoxy-3-methylbutoxy)phenyl]porphinato]zinc(II)]ethyne (**12**), bis[(2,2'-5,10,15,20-tetraphenylporphinato)zinc(II)]ethyne (**13**), [(2-5,10,15,20-tetraphenylporphinato)zinc(II)]-[5'-10'20'-bis[4-(3-methoxy-3-methylbutoxy)phenyl]porphinato]zinc(II)]ethyne (**14**), [(2-5,10,15,20-tetrakis(trifluoromethyl)porphinato)zinc(II)]-[5'-10'20'-bis[4-(3-methoxy-3-methylbutoxy)phenyl]porphinato]zinc(II)]ethyne (**15**), [(2-5,10,15,20-tetrakis(trifluoromethyl)porphinato)zinc(II)]-[2'-5',10',15',20'-tetraphenylporphinato]zinc(II)]ethyne (**16**), and bis-[(2-5,15-(trifluoromethyl)-10,20-diphenylporphinato]zinc(II)]ethyne (**17**) were all fabricated in a straightforward fashion.^{30,31} Ethyne-bridged, bis[(porphinato)zinc(II)] species **12**–**18** were converted to their corresponding 1,2-phenylene-bridged bis[(porphinato)metal] compounds (Scheme 2) via a Co-templated cycloaddition with 1,6-heptadiyne; note that in these species (**1**–**7**), both macrocycle electronic structure and the

Scheme 2^a

^aGeneral reaction conditions employed: (i) $\text{Co}_2(\text{CO})_8$ (1 equiv), toluene/dioxane 5:1, 100 °C, 10 min; (ii) 1,6-heptadiyne (20 equiv), $\text{Co}_2(\text{CO})_8$ (1 equiv), 5 mL of toluene, added 17 h dropwise.

(porphinato)metal–(porphinato)metal linkage topology are varied systematically.

The [2+2+2] cycloaddition protocol was optimized for substrate **12**, which was converted to 5,6-bis[(5',5''–10',20'-bis[4-(3-methoxy-3-methylbutoxy)phenyl]porphinato)zinc(II)]indane (**1**) in 94% yield; these reaction conditions were employed for all ethyne-bridged porphyrin substrates in this study. It is well known that such metal-mediated cycloaddition

transformations are sensitive to both alkyne steric^{32–34,42,45–48} and electronic^{45,49} properties; hence, the range of yields observed for this series is not surprising, given that reaction time was held essentially constant. Interestingly, in most cases, more than 90% of the porphyrin reactant was accounted for either as product or recovered starting material (see Experimental Section); as deleterious side reactions appear lacking, it is likely that each of these transformations can be optimized individually to give similarly high yields as that observed for the **12**-to-**1** conversion.

While 1,2-phenylene-bridged bis[(porphinato)metal] compounds analogous to meso–meso bridged **1** and meso– β bridged 5-[(2'–5',10',15',20'-tetraphenylporphinato)zinc(II)]–6-[(5''–10'',20''-bis[4-(3-methoxy-3-methylbutoxy)phenyl]porphinato)zinc(II)]indane (**3**) have been reported,²³ 5,6-bis[(2'–5',10',15',20'-tetraphenylporphinato)zinc(II)]indane (**2**) and 5,6-bis[(2'–5',10',15',20'-tetrakis(trifluoromethyl)porphinato)zinc(II)]indane (**7**) serve as archetypal examples of β – β bridged cofacial porphyrin structures. Products 5-[(2'–5',10',15',20'-tetrakis(trifluoromethyl)porphinato)zinc(II)]–6-[(5''–10'',20''-bis[4-(3-methoxy-3-methylbutoxy)phenyl]porphinato)zinc(II)]indane (**4**), 5-(2'–5',10',15',20'-[tetrakis(trifluoromethyl)porphinato)zinc(II)]–6-[(2''–5'',10'',15'',20''-tetraphenylporphinato)zinc(II)]indane (**5**), 5,6-bis[(2'–5',15'-(trifluoromethyl)-10',20'-diphenylporphinato)zinc(II)]indane (**6**), and **7** are the first examples of cofacial bis[(porphinato)metal] complexes that possess perfluoroalkyl-substituted macrocycles; furthermore, these species highlight that this synthetic strategy enables extensive regulation of both the extent of macrocycle–macrocycle electronic asymmetry and the energetics of the cofacial (porphinato)metal frontier orbitals (vide infra).

The nature of interporphyrin π – π interactions will play a pivotal role in determining the electronic properties of cofacial bis[(porphinato)metal] complexes and will be determined by the indane-to-porphyrin macrocycle linkage topology (Figure 1). Unlike 1,2-phenylene-bridged cofacial porphyrin structures with meso–meso connectivity,^{19,23,42,50} two possible structural conformations can be manifest in meso– β and β – β bridged systems. In the meso– β bridging motif highlighted in **3** and **4** (Figure 1A), the two enantiomers possess equivalent π -cofacial electronic interactions. In contrast, disparate π – π interactions are evident for the two β – β bridged atropisomers possible for **2**, **5**, **6**, and **7** (Figure 1B). Both ¹H and ¹⁹F NMR analyses of each of these β – β bridged bis[(porphinato)zinc(II)] complexes confirm that only one atropisomer exists in solution at room temperature (see Experimental Section), presumably due to the fact that the eclipsed *Z* isomer possesses augmented steric strain relative to the *E* configuration (Figure 1B).

(43) Samuels, E.; Shuttleworth, R.; Stevens, T. S. *J. Chem. Soc. C* **1968**, 145–147.

(44) Callot, H. J. *Bull. Soc. Chim. Fr.* **1974**, 1492.

(45) Dickson, R. S.; Fraser, P. J. *Adv. Organomet. Chem.* **1974**, *12*, 323–377.

(46) Hillard, R. L., III; Vollhardt, K. P. C. *J. Am. Chem. Soc.* **1977**, *99*, 4058–4069.

(47) Berris, B. C.; Hovakeemian, G. H.; Lai, Y.-H.; Mestdagh, H.; Vollhardt, K. P. C. *J. Am. Chem. Soc.* **1985**, *107*, 5670–5687.

(48) Chiusoli, G. P.; Costa, M.; Zhou, Z. *Gazz. Chim. Ital.* **1992**, *122*, 441–449.

(49) It is known that $\text{Co}_2(\text{CO})_8$ forms more stable complexes with alkynes containing electron-withdrawing substituents (see ref 45); a less reactive cobalt intermediate is likely to be at least partly responsible for the decreased product yields that are apparent in cycloaddition reactions involving perfluoroalkyl-substituted porphyrin species.

(50) Shimazaki, Y.; Takesue, H.; Chishiro, T.; Tani, F.; Naruta, Y. *Chem. Lett.* **2001**, 538–539.

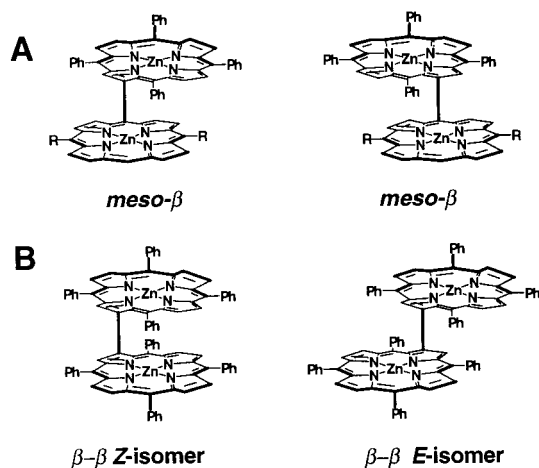
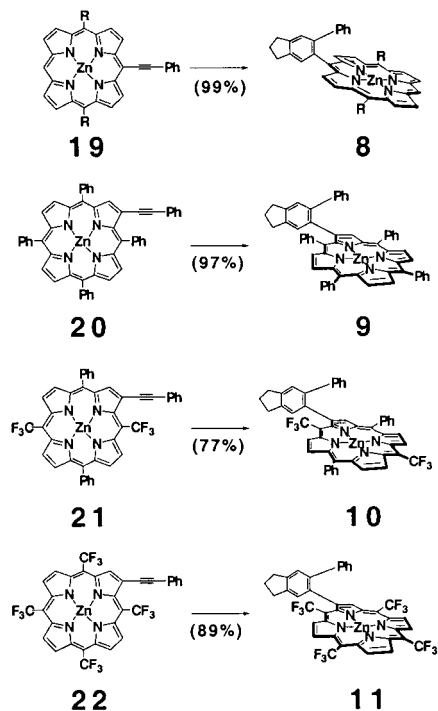


Figure 1. Illustration of the possible meso- β enantiomers and β - β atropisomers in cofacial bis[(porphinato)zinc(II)] complexes featuring these linkage topologies.

Scheme 3^a



^aGeneral reaction conditions employed: (i) $\text{Co}_2(\text{CO})_8$ (1 equiv), toluene/dioxane 5:1, 100 °C, 10 min; (ii) 1,6-heptadiyne (10 equiv), 5 mL of toluene, added 90 min dropwise.

To facilitate the analyses of spectroscopic and potentiometric data for these cofacial bis[(porphinato)zinc(II)] complexes, an appropriate set of monomeric standards was synthesized. 5-(6-Phenyl)indanyl-derivatized porphyrin monomers (Scheme 3) were constructed via palladium-catalyzed cross-coupling of ethynylbenzene with meso- or β -brominated porphyrin precursors, followed by cycloaddition with 1,6-heptadiyne; these compounds (**8–11**, Scheme 3) were utilized as analytical benchmarks in lieu of simple 5,15- or 5,10,15,20-derivatized porphyrins.

Electronic Spectroscopy. Figure 2 depicts the electronic absorption spectra of cofacial bis[(porphinato)zinc(II)] complexes **1–7**; absorption and emission data for these species are summarized in Table 1. A strongly allowed exciton band, blue-shifted with respect the Soret band of the simple (porphinato)-

zinc(II) building block, is a spectral hallmark of cofacial bis[porphyrin] compounds having modest porphyrin–porphyrin interplanar separations.^{51–53} The λ_{max} of the Soret band of meso–meso bridged dimer **1** is shifted hypsochromically 634 cm^{-1} in comparison to benchmark **8**. In contrast, β - β bridged dimer **2** is blue-shifted by only 166 cm^{-1} versus benchmark **9**. Note, however, that electron-poor β - β bridged **7** displays strong exciton coupling, with the λ_{max} of its Soret band hypsochromically shifted by 1253 cm^{-1} relative to **11**. These data indicate that the relative degree of exciton coupling between porphyrin units is not dependent solely upon macrocycle–macrocycle relative orientation; the nature of the macrocycle frontier orbitals clearly plays a role as well (vide infra). The general electronic spectral features peculiar to cofacial [(porphinato)zinc(II)] complexes possessing either asymmetric connectivity or electronically disparate macrocycle units have been discussed previously.²³

Electrochemical Studies. A large number of dimeric porphyrin and (porphinato)zinc compounds bridged cofacially by rigid aryl spacers have been reported,^{16–22} and their electronic properties relative to simple porphyrinic monomers have been discussed.⁵⁴ Each of these previously reported systems were connected via the macrocycle meso positions, and the observed frontier orbital destabilization evident in the cofacial bis[(porphinato)metal] complex relative to the corresponding monomeric chromophore was attributed to electrostatic repulsions between the π -systems of the closely stacked porphyrin macrocycles.⁵⁴ Due to the symmetry of the porphyrin macrocycle's frontier molecular orbitals, differences in both macrocycle–macrocycle connectivity and electronic structure should have a profound impact on the nature of electronic interactions in such π -stacked structures. Potentiometric studies of the series of cofacial structures reported herein enable quantitative assessment of the extent to which these factors impact the frontier orbital energy levels of face-to-face bis[(porphinato)metal] compounds.

Structural studies evince that the cofacial orientation of 1,2-phenylene-bridged bis[(porphinato)metal] compounds is dependent strongly upon the solvent system used to obtain X-ray-quality crystals.^{19,23,42,50} When noncoordinating solvents are used, such structures adopt largely coplanar conformations; in contrast, when coordinating solvents are utilized, X-ray crystallographic studies show that cofacial bis[(porphinato)metal] species express open conformations possessing large dihedral angles between the porphyrin least-squares planes. Because coordinating solvents were utilized in our electrochemical studies, we consider only the open cofacial conformation in the analyses of these data.

In a 1,2-phenylene-bridged bis[(porphinato)zinc(II)] structure, a number of sub-van der Waals contacts are enforced, assuming a typical dihedral angle of 60° between macrocycle least-squares planes, as demonstrated by both computational studies and X-ray crystallographic analyses.^{23,42,55} For example, computational modeling (Supporting Information) indicates the closest of these cofacial contacts for a meso–meso bridged structure are at the

(51) Kasha, M.; Rawls, H. R.; El-Bayoumi, M. A. *Pure Appl. Chem.* **1965**, *11*, 371–392.

(52) Chang, C. K. *Adv. Chem. Ser.* **1979**, No. 173, 162–177.

(53) Hunter, C. A.; Sanders, J. K. M.; Stone, A. J. *Chem. Phys.* **1989**, *133*, 395–404.

(54) Le Mest, Y.; L'Her, M.; Hendricks, N. H.; Kim, K.; Collman, J. P. *Inorg. Chem.* **1992**, *31*, 835–847.

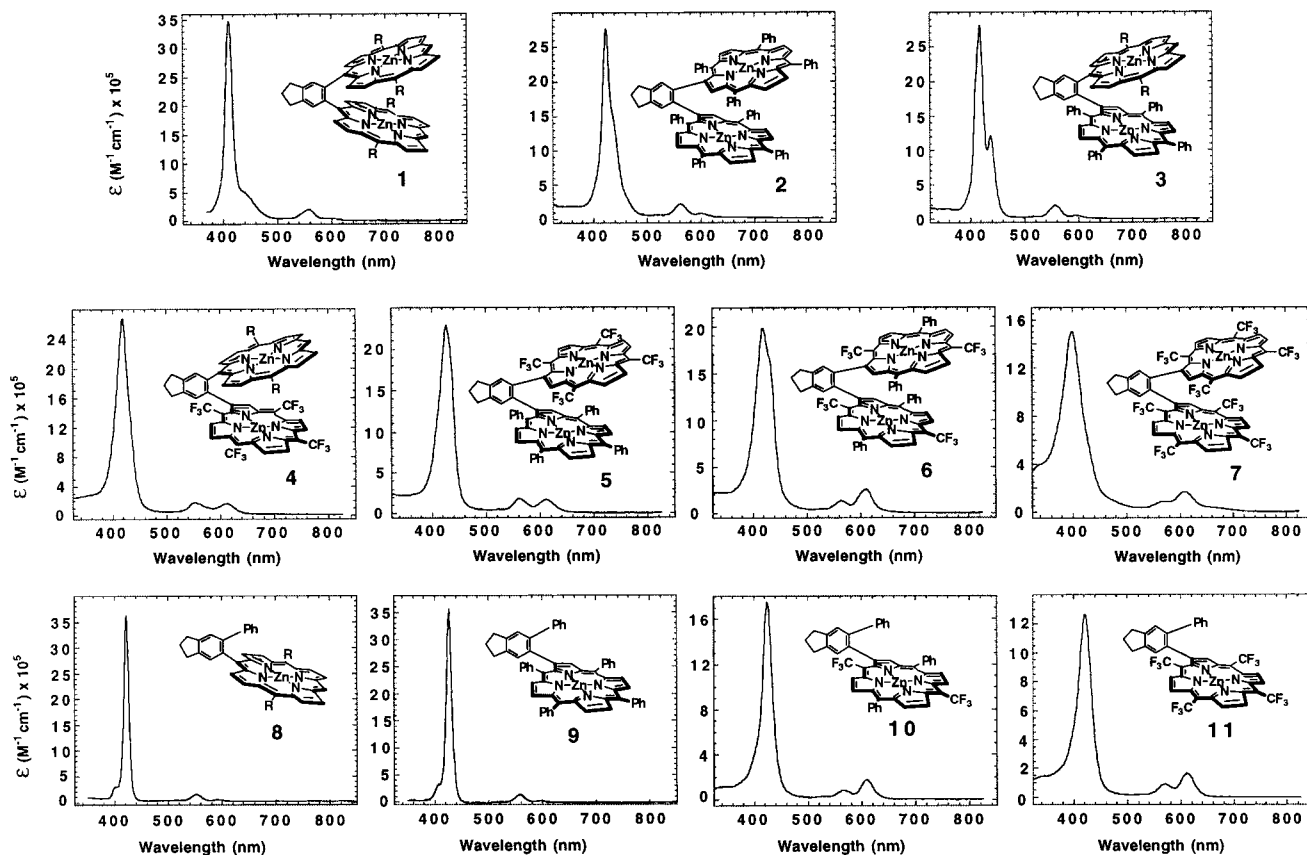


Figure 2. Electronic absorption spectra of 5,6-bis[(porphinato)zinc(II)]indane complexes **1–7** and 5-phenyl-6-[(porphinato)zinc(II)]indane compounds **8–11** recorded in THF solvent ($T = 23\text{ }^{\circ}\text{C}$).

Table 1. Prominent Absorption and Emission Bands of 5,6-Bis[(porphinato)zinc(II)]indane and 5-Phenyl-6-[(porphinato)zinc(II)]indane Complexes, Recorded in THF Solvent

compd	electronic absorption						fluorescent emission	
	B-band region			Q-band region			λ (nm)	ν (cm^{-1})
	λ (nm)	ν (cm^{-1})	$\log(\epsilon)$	λ (nm)	ν (cm^{-1})	$\log(\epsilon)$	λ (nm)	ν (cm^{-1})
1	411	24 331	5.54	558	17 921	4.32	611	16 367
	434	23 041	4.74	589	16 978	3.72	657	15 521
				599	16 695	3.71		
2	424	23 585	5.44	561	17 825	4.34	617	16 207
				599	16 694	3.92	662	15 106
3	418	23 923	5.45	555	18 018	4.31	612	16 340
	438	22 831	5.09	595	16 807	3.76	655	15 267
4	418	23 923	5.43	555	18 018	4.26	639	15 649
				612	16 340	4.22	684	14 620
5	426	23 474	5.36	562	17 794	4.83	629	15 898
				612	16 340	4.22		
6	419	23 866	5.13	564	17 730	4.12	625	16 000
				610	16 393	4.41		
7	399	25 063	5.18	570	17 544	3.94	633	15 798
				608	16 447	4.23		
8	422	23 697	5.56	552	18 116	4.21	601	16 639
				592	16 892	3.57	649	15 408
9	427	23 419	5.55	558	17 921	4.16	611	16 367
				597	16 750	3.92	655	15 267
10	424	23 585	5.24	566	17 668	3.94	635	15 748
				608	16 447	4.24		
11	420	23 810	5.10	570	17 544	3.96	635	15 748
				612	16 340	4.22		

C3, C5, and C7 positions of the macrocycles, which possess average interplanar atom–atom separations (C3–C3', C5–C5', C7–C7') of less than 3.0 Å. Similar sub-van der Waals contacts are evident in the meso- β , and β - β structures (meso- β , C3–

C5', C5–C3'; β - β , C2–C4', C4–C2'). Note also that each cofacial bis(porphyrin) linkage topology shows additional macrocycle–macrocycle atom–atom contacts at the van der Waals separation distance of ~ 3.4 Å (meso–meso, C4–C4', C6–C6'; meso- β , C4–C4', C6–C2'; β - β , C3–C3'). Other porphyrin atomic positions manifest atom–atom interplanar separations exceeding π -contact distances. For example, at a 60° dihedral angle between the macrocycle least-squares planes, the average N1–N1' and N2–N2' separations for the meso–meso linked structure are ~ 4.9 Å; thus, our first-order analysis of the electronic interactions that fix the frontier orbital energy levels of 5,6-indanyl-bridged cofacial (porphinato)zinc(II) structures focus on these positions of close contact between the two macrocycle planes.⁵⁶

Cyclic voltammetric data for the 5,6-bis[(porphinato)zinc(II)]indane and 5-phenyl-6-[(porphinato)zinc(II)]indane complexes are presented in Table 2; exemplary cyclic voltammetric responses for these species are shown in the Supporting Information. It is evident from the comparison of the electron-rich bis[(porphinato)zinc(II)] species **1**, **2**, and **3** that macrocycle–macrocycle connectivity influences frontier orbital energy levels. Compound **1** (Figure 3A) displays oxidative and reductive cyclic voltammetric processes consistent with those reported

(55) Cofacial bis[(porphinato)zinc(II)] species were modeled using the CaChE molecular mechanics package; the porphyrin macrocycles were restricted to planar conformations in which the interporphyrin dihedral angle was fixed at 60° (see Supporting Information). The interporphyrin separations predicted by these structural models were within ± 0.1 Å of the distances manifest in the X-ray crystallographic structures of open meso–meso linked, 1,2-phenylene bridged cofacial porphyrin compounds.^{23,42,50}

(56) For a complete listing of interporphyrin atom–atom contact distances used in this analysis, see the Supporting Information.

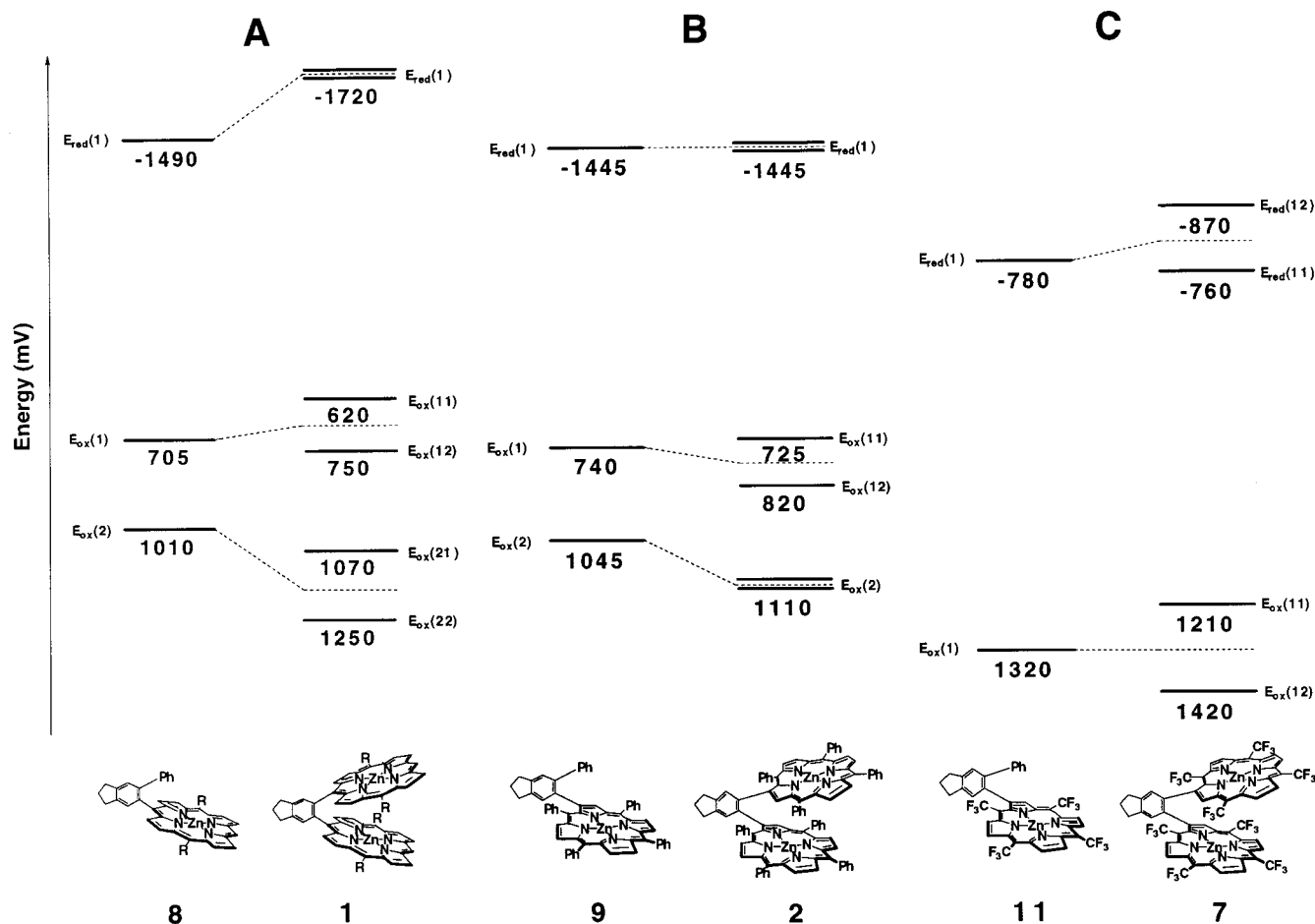


Figure 3. Potentiometrically determined relative frontier molecular orbital energy levels for the following: (A) 5-phenyl-6-[(5'-10',20'-bis[4-(3-methoxy-3-methylbutoxy)phenyl]porphinato)zinc(II)]indane (**8**) and 5,6-bis[(5',5''-10',20'-bis[4-(3-methoxy-3-methylbutoxy)phenyl]porphinato)zinc(II)]indane (**1**); (B) 5-phenyl-6-[(2'-5',10',15',20'-tetraphenylporphinato)zinc(II)]indane (**9**) and 5,6-bis[(2'-5',10',15',20'-tetraphenylporphinato)zinc(II)]indane (**2**); and (C) 5-phenyl-6-[(2'-5',10',15',20'-tetrakis(trifluoromethyl)porphinato)zinc(II)]indane (**11**) and 5,6-bis[(2'-5',10',15',20'-tetrakis(trifluoromethyl)porphinato)zinc(II)]indane (**7**).

Table 2. Comparative Cyclic Voltammetric Data of the 5,6-Bis[(porphinato)zinc(II)]indane Complexes and 5-Phenyl-6-[(porphinato)zinc(II)]indane Benchmarks^a

compd	$E_{1/2}$ (mV)			
	ZnP/ZnP ⁺	ZnP ⁺ /ZnP ²⁺	ZnP/ZnP ²⁺	ZnP ⁻ /ZnP
1	620, 750	1070, 1250		-1720 ^b
2	725, 820	1110 ^b		-1445 ^b
3	735, 805	1080, 1250		-1740 ^b
4	710	990	1420 ^b	-1070, -1650
5	740	995	1415 ^b	-980, -1455
6			1085, ^b 1250 ^b	-1040, -1290
7			1210, ^b 1420 ^b	-775, -890
8	705	1010		-1490
9	740	1045		-1445
10			1090 ^b	-985
11			1320 ^b	-780

^a Experimental conditions: solvent, benzonitrile; [porphyrin] = 1–2 mM; [TBAClO₄] = 0.1 M; scan rate, 100–1000 V/s; reference electrode, Ag wire. $E_{1/2}$ values reported are relative to SCE; the ferrocene/ferrocenium redox couple (0.43 vs SCE, benzonitrile) was used as the internal standard. ^b Signifies a 2e redox step. See Figures 3 and 4.

for meso–meso bridged cofacial (porphinato)zinc(II) dimers.^{19,54} Note that the initial anodic step of the first oxidative process of **1** is destabilized by 85 mV relative to monomeric **8**, while the second step of the first oxidative process is stabilized by 45 mV relative to this benchmark (Table 2). These observed potentiometric shifts with respect to the (porphinato)zinc(II)

monomer have been commonly attributed to electrostatically driven destabilization of the HOMO in the neutral bis[(porphinato)zinc(II)] complex and the fact that the cation radical state of the dimer gains added stability due to electronic delocalization.⁵⁴ Consistent with previously reported electrochemical analyses,⁵⁴ **1**'s initial cathodic redox process is shifted substantially (–230 mV) to more negative potential relative to reference monomer **8**.

Both β – β and meso– β bridged dimers **2** and **3**, which also feature exclusively meso-aryl substituents, differ markedly from **1** with respect to the degree that their frontier orbitals are perturbed relative to reference (porphinato)zinc(II) complexes. The initial step of **2**'s first oxidative process (Figure 3B) is shifted only modestly (15 mV) relative to reference **9**, while the second anodic step is strongly stabilized by 80 mV (Table 2). In further contrast to the cyclic voltammetric data obtained for **1**, the potential of **2**'s first reductive process is unchanged versus that determined for reference monomer **7**. Meso– β bridged dimer **3** (Figure 4A) displays similar trends in its first oxidation process: the potential of **3**'s initial anodic step differs little from the one-electron (1e) oxidation potentials determined for **8** and **9**, while its second anodic step is stabilized on the order of 100 mV. Notably, in contrast to β – β bridged **2**, **3**'s first reductive process is destabilized relative to its monomeric

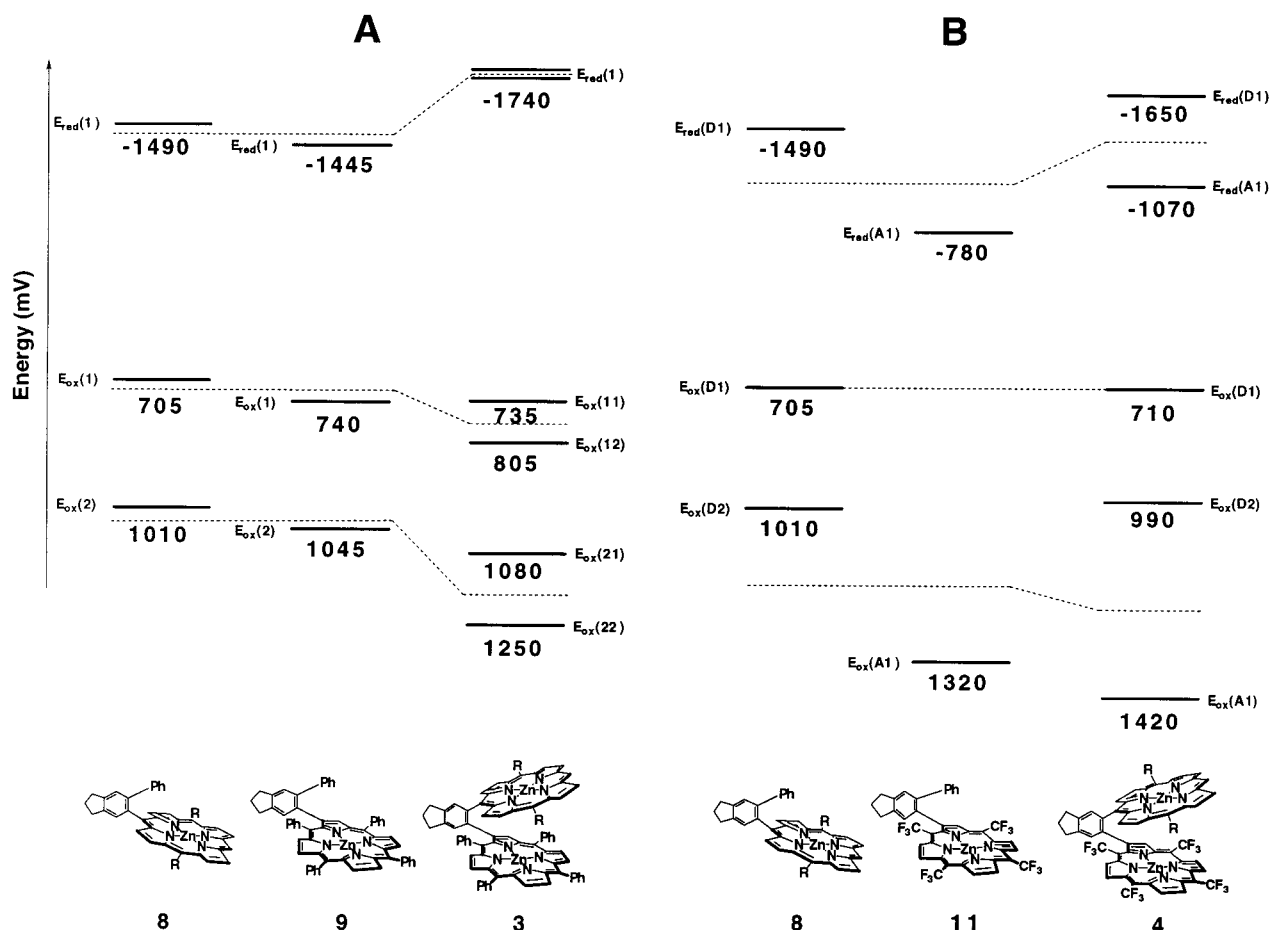


Figure 4. Potentiometrically determined relative frontier molecular orbital energy levels for the following: (A) 5-phenyl-6-[(5'-10',20'-bis[4-(3-methoxy-3-methylbutoxy)phenyl]porphinato)zinc(II)]indane (**8**), 5-phenyl-6-[(2'-5',10',15',20'-tetraphenylporphinato)zinc(II)]indane (**9**), and 5-[(2'-5',10',15',20'-tetraphenylporphinato)zinc(II)]-6-[(5''-10'',20''-bis[4-(3-methoxy-3-methylbutoxy)phenyl]porphinato)zinc(II)]indane (**3**); and (B) 5-phenyl-6-[(5'-10',20'-bis[4-(3-methoxy-3-methylbutoxy)phenyl]porphinato)zinc(II)]indane (**8**), 5-phenyl-6-[(2'-5',10',15',20'-tetrakis(trifluoromethyl)porphinato)zinc(II)]indane (**11**), and 5-[(2'-5',10',15',20'-tetrakis(trifluoromethyl)porphinato)zinc(II)]-6-[(5''-10'',20''-bis[4-(3-methoxy-3-methylbutoxy)phenyl]porphinato)zinc(II)]indane (**4**).

(porphinato)zinc(II) benchmarks to a degree similar (~ -275 mV) to that evinced for meso-meso bridged **1** (Table 2).

The relative differences between the respective frontier orbital energies of **1**, **2**, and **3** can be explained qualitatively using a simple through-space interaction model that considers the relevant interactions of the classic, macrocycle-localized Gouterman four orbitals (Figure 5).⁵⁷ Each of the (porphinato)zinc(II) units of face-to-face porphyrin compounds **1**, **2**, and **3** possess HOMOs with a_{2u} symmetry; this orbital has significant electron density at its meso and N pyrrolyl positions. Qualitative evaluation of the extent of out-of-phase orbital interactions between macrocycle a_{2u} HOMOs in **1**, **2**, and **3** as a function of bridging connectivity provides a rationale for the observed relative energies of the frontier orbitals of these complexes.

Figure 6 identifies the nature of the highest lying filled-filled interaction as a function of macrocycle-macrocycle connectivity and the symmetries of the HOMOs of the constituent (porphinato)zinc(II) units of the cofacial porphyrin complex. The extent of wave function overlap of the HOMOs of the two (porphinato)zinc(II) units in the regions of conformational space that feature sub-van der Waals contacts between porphyrin macrocycles (assuming a 60° dihedral angle between the

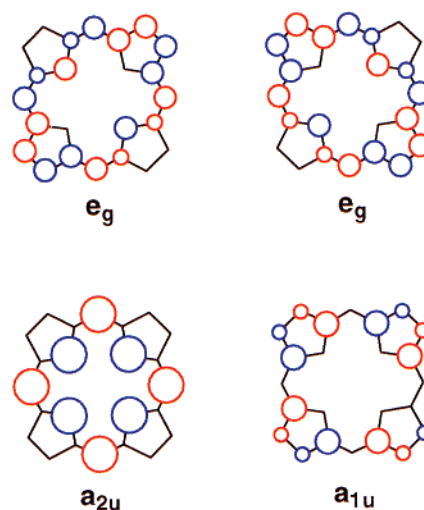


Figure 5. (Porphinato)metal frontier orbitals described by Gouterman.⁵⁷ The red and blue coding denotes opposite phases of the porphyrin p orbital wave functions, and circle size reflects approximate relative atom-centered electron densities.

porphyrin least-squares plane)⁵⁵ are highlighted in Figure 6, with solid red/blue denoting out-of-phase orbital overlap and solid purple indicating in-phase orbital overlap. As depicted in Figure 6A, the meso-meso linked, 5,6-indanyl-bridged cofacial bis-

(57) Gouterman, M. In *The Porphyrins*; Dolphin, D., Ed.; Academic Press: New York, 1978; Vol. 3, pp 1-165.

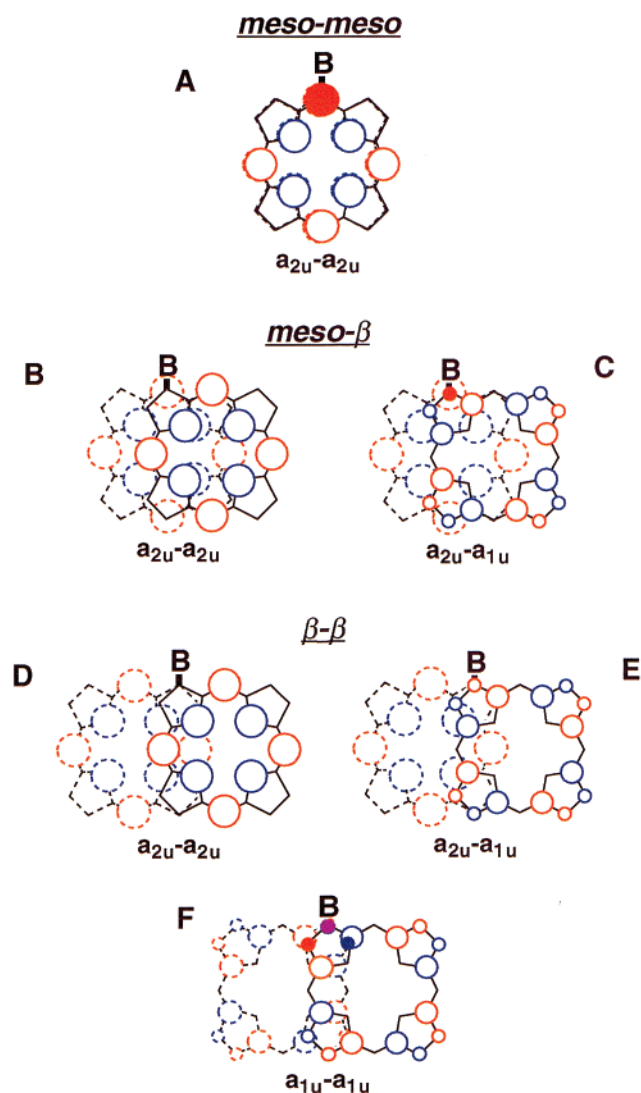


Figure 6. Qualitative depiction of (porphinato)zinc(II)–(porphinato)zinc(II) HOMO–HOMO interactions occurring within van der Waals contact in cofacial porphyrin systems possessing idealized 60° dihedral angles between porphyrin least-squares planes.⁵⁵ The label B indicates the connectivity to the 5,6-indanyl bridge. Color coding: red/blue, out-of-phase orbital overlap; purple, in-phase orbital overlap.

[(porphinato)zinc(II)] **1** system enforces significant a_{2u} – a_{2u} out-of-phase orbital overlap; note that, at the meso carbon atoms connected to the 5- and 6-indane positions, this unfavorable electronic interaction occurs at a distance substantially less than van der Waals contact and is thus likely a primary determinant of the extensive destabilization of the compound **1** HOMO relative to that of monomeric **8**. In contrast, there is little sub-van der Waals out-of-phase orbital overlap at the bridging β positions of dimer **2** (Figure 6D); as a result, this face-to-face porphyrin compound does not display significant destabilization of its HOMO level with respect to benchmark **9**. Similarly, due to minimal overlap of the (porphinato)zinc(II) a_{2u} HOMOs connected via a meso– β linkage topology (Figure 6B), **3** also evinces no measurable destabilization of its HOMO energy level (Figure 4A) relative to that determined for its (porphinato)zinc(II) building blocks. Related connectivity-dependent electronic interactions have been elucidated for various classes of conjugated linear porphyrin arrays.^{30,31,58}

Each of these bis[(porphinato)zinc(II)] compounds possesses strongly stabilized second steps of their first oxidative processes, a commonly observed characteristic of cofacial porphyrin systems.^{19,54} It is interesting to note that the degree of stabilization (meso–meso (130 mV) > meso– β (95 mV) > β – β (70 mV)) observed for the second steps of the first oxidative process for **1**, **2**, and **3** coincides with the extent of (porphinato)zinc–(porphinato)zinc HOMO–HOMO wave function overlap (Supporting Information) for a coplanar bis[(porphinato)zinc(II)] structure. This analysis is consistent with the postulate that stabilization of the second anodic step of the first oxidative process for cofacial porphyrin compounds derives from substantial electronic delocalization made possible in electrochemically generated $(PZn)_2^+$ species.⁵⁴

Disparate frontier orbital energies of the constituent (porphinato)zinc(II) units play a key role in determining the observed anodic cyclic voltammetric responses for electronically asymmetric bis[(porphinato)zinc(II)] complexes **4** and **5** (Table 2, Figure 4). The initial anodic steps of the first oxidative processes for the respective meso– β and β – β connected structures **4** and **5** are unperturbed relative to their electron-rich monomeric components, despite the fact that for meso– β bridged **4** there exists out-of-phase overlap of the HOMOs of the constituent (porphinato)zinc(II) moieties in regions of space that feature sub-van der Waals porphyrin–porphyrin contacts (Figure 6C). This effect has its genesis in the fact that the HOMO energy levels of the (porphinato)zinc(II) units in these cofacial structures differ by more than 600 mV (Figure 4B). Notably, electronic delocalization effects are clearly apparent in the third oxidation for **4** and **5**, with the anodic process associated primarily with the tetrakis(perfluoroalkyl)porphyrin component stabilized ~ 100 mV ($E_{1/2}(PZn)_2^{2+/3+} = 1420$ mV (**4**); $E_{1/2}(PZn)_2^{2+/3+} = 1415$ mV (**5**)) relative to the initial oxidation of benchmark **11** ($E_{1/2}(PZn)^{2+/3+} = 1320$ mV; see Table 2 and Figure 4B).

It is interesting to compare the redox profile of β – β connected dimer **7** (Figure 3C), composed of (porphinato)zinc(II) units having a_{1u} HOMOs^{36,37,59} with dimer **2** (Figure 3B), which possesses (porphinato)zinc(II) components with a_{2u} HOMOs and an equivalent macrocycle–macrocycle linkage topology. Unlike **2**, **7** shows strong destabilization of its HOMO level with respect to its monomeric benchmark complex **11**. In the region of sub-van der Waals macrocycle–macrocycle contact (Figure 6D) electron-rich β – β linked cofacial porphyrin dimer **2** shows minimal overlap of the building block (porphinato)zinc(II) HOMO wave functions; in contrast, electron-poor β – β linked dimer **7** shows significant out-of-phase (porphinato)zinc–(porphinato)zinc a_{1u} – a_{1u} overlap in this region of space (Figure 6F), giving rise to substantial electronic interactions that result in destabilization of the HOMO of the cofacial bis[(porphinato)zinc(II)] complex.

The relative energy levels of the lowest unoccupied molecular orbitals of these cofacial bis[(porphinato)metal] systems can be rationalized in a manner analogous to that used to explain differences in the observed anodic electrochemistry of these species (Figure 7). Note that, in contrast to the case for the filled states, the extent of LUMO destabilization in the bis[(porphinato)zinc(II)] complex will correlate with the extent of in-phase

(58) Yang, S. I.; Seth, J.; Balasubramanian, T.; Kim, D.; Lindsey, J. S.; Holten, D.; Bocian, D. F. *J. Am. Chem. Soc.* **1999**, *121*, 4008–4018.

(59) Moore, K. T.; Fletcher, J. T.; Therien, M. J. *J. Am. Chem. Soc.* **1999**, *121*, 5196–5209.

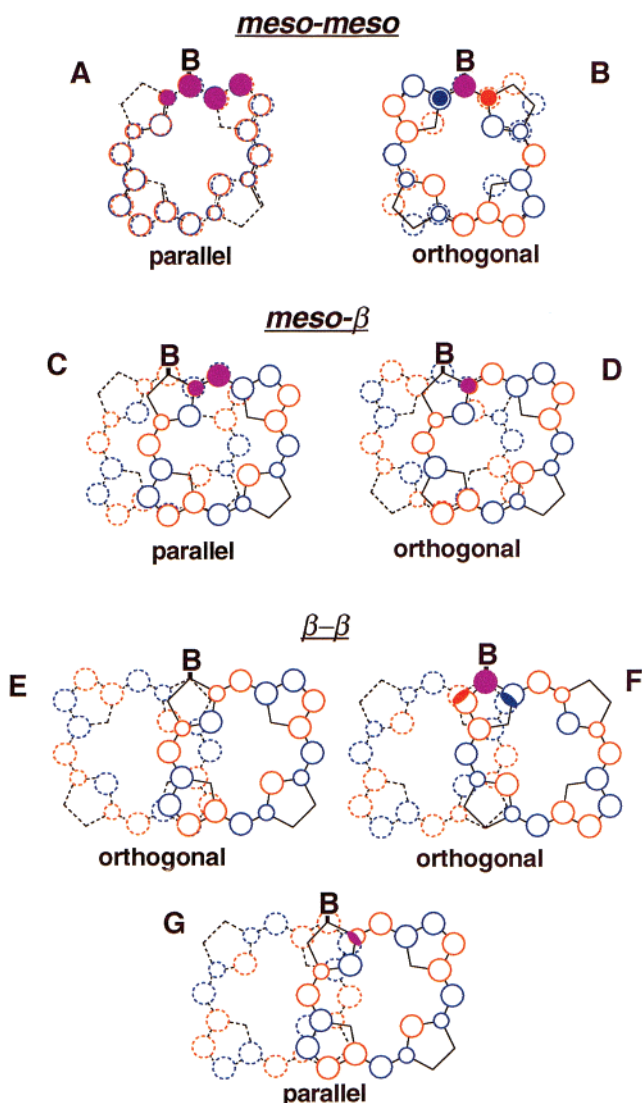


Figure 7. Qualitative depiction of (porphinato)zinc(II)–(porphinato)zinc(II) LUMO–LUMO interactions occurring within van der Waals contact in cofacial porphyrin systems possessing idealized 60° dihedral angles between porphyrin least-squares planes.⁵⁵ The label B indicates the connectivity to the 5,6-indanyl bridge. Color coding: see Figure 6.

macrocycle–macrocycle LUMO–LUMO interactions; such orbital overlap effects further augmentation of the already large porphyrin–porphyrin repulsive interactions, causing uniform destabilization of all occupied orbital energy levels.

The strong destabilization of the LUMO energy observed for meso–meso bridged **1** is consistent with that delineated for other cofacial porphyrin structures having meso–meso connectivity.⁵⁴ While cathodic potentiometric data for stacked aromatic structures are sparse, it is important to note that the few literature examples of π -cofacial arene one-electron reduction potentials follow the trend delineated for meso–meso bridged cofacial bis(porphyrins). Particularly relevant in this regard is the body of data that shows that flavin moieties involved in π -stacking interactions with other aromatics display flavin⁻⁰ potentials that decrease precipitously with increasing electron-releasing character of the π -stacked arene; this behavior has been observed both in flavoenzymes^{60,61} and in simple model compounds.⁶²

(60) Zhou, Z.; Swenson, R. P. *Biochemistry* **1996**, *35*, 15980–15988.

Note that, for meso–meso bridged cofacial porphyrin complexes, significant in-phase (porphinato)metal–(porphinato)metal wave function overlap exists in the region of sub-van der Waals contact, regardless of whether the primary electronic interaction in the LUMO of the face-to-face structure involves parallel (Figure 7A) or orthogonal (Figure 7B) components of the e_g sets of the (porphinato)zinc(II) units (Figure 5). Similarly, meso– β bridged structures also display significant in-phase wave function overlap of the constituent (porphinato)zinc(II)-based LUMO wave functions in the region of van der Waals contact (Figure 7C,D). As such, meso– β bridged **3**, which is composed of electronically similar meso-aryl (porphinato)zinc(II) units, displays a similarly large LUMO destabilization as was observed for meso–meso bridged **1**. It is interesting to note that the insightful Hunter–Sanders electrostatic model,⁶³ which captures the essence of most essential trends with respect to the electronic structure of π -stacked aromatics, predicts that repulsive electrostatic interactions should be considerably less for the meso– β linkage topology with respect to that manifest by a meso–meso bridge at equivalent interplanar separations; the fact that this trend is not manifest in the potentiometric data of **1** and **3** further underscores that the relative phase relationships of the frontier orbitals of the component aromatic units is an additional factor that need also be considered in such theoretical analyses.

In contrast, electronically symmetric β – β bridged **2** and **7** each display no destabilization of their LUMO energy levels (Figure 3), suggesting that insignificant overlap of the (porphinato)zinc(II) monomer-based e_g symmetric LUMO wave functions is manifest in the region of sub-van der Waals contact. Examination of the possible modes of interaction between the orthogonal and parallel e_g wave function components shows that two combinations (Figure 7F and G) result in partial wave function overlap in the region of sub-van der Waals contact, while one combination of (porphinato)zinc(II)-localized orthogonal e_g wave functions (Figure 7E) results in a cofacial bis-[(porphinato)zinc(II)] LUMO having no electronic interaction between the porphyrin units. Potentiometric data are thus consistent with the orbital interaction shown in Figure 7E being relevant to the description of the radical anion states of **2** and **7**.

Notably, the LUMOs for both cofacial bis[(porphinato)zinc(II)] complexes **4** and **5**, which feature significant macrocycle–macrocycle electronic asymmetry, show similar degrees of destabilization with respect to the potentiometrically determined LUMO energy level of the [5,10,15,20-tetrakis(perfluoroalkyl)porphinato]zinc(II) benchmark **11**. The cathodic potentiometric data obtained for meso– β linked **4** (Figure 4, Table 2) follow the trend expected for this macrocycle–macrocycle linkage topology (Figure 7C,D) with the measured $E_{1/2}(\text{PZn})^{-/0}$ value destabilized 290 mV relative to the $E_{1/2}(\text{PZn})^{-/0}$ potential (Figure 7, Table 2). Interestingly, β – β linked **5** displays an $E_{1/2}(\text{PZn})^{-/0}$ value (Table 2) destabilized by 200 mV relative to **11**; this potentiometric behavior contrasts that elucidated for β – β bridged **2** and **7** (vide supra), in which the $E_{1/2}(\text{PZn})^{-/0}$ values are unperturbed relative to their respective standards **9**

(61) Pellett, J. D.; Becker, D. F.; Saenger, A. K.; Fuchs, J. A.; Stankovich, M. T. *Biochemistry* **2001**, *40*, 7720–7728.

(62) Breinlinger, E. C.; Rotello, V. M. *J. Am. Chem. Soc.* **1997**, *119*, 1165–1166.

(63) Hunter, C. A.; Saunders, J. K. M. *J. Am. Chem. Soc.* **1990**, *112*, 5525–5534.

(64) Chang, C. K. *J. Heterocycl. Chem.* **1977**, *14*, 1285–1288.

(65) Eaton, S. S.; Eaton, G. R.; K., C. C. *J. Am. Chem. Soc.* **1985**, *107*, 3177–3184.

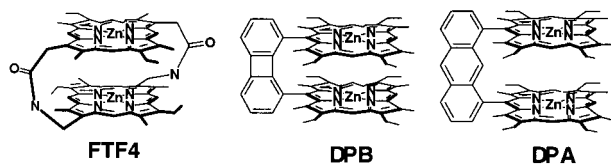


Figure 8. Classic examples of the electron-rich cofacial bis[(porphinato)-zinc(II)] architecture.^{1,2,4,5,16,20,52,64,65} Potentiometric data for these species⁵⁴ are used as benchmarks in Figure 9.

and **11** (Figure 6, Table 2). While the origin of this behavior is an open question, it likely derives from the strong electronic asymmetry inherent to **4** and **5**. As noted above, cyclic voltammetric data argue that the orbital interactions displayed in Figure 7E describe the essential characteristics of the LUMO for electronically symmetric cofacial bis[(porphinato)zinc(II)] compounds **2** and **7**. Because the HOMO and LUMO energy levels of [5,10,15,20-tetrakis(perfluoroalkyl)porphinato]zinc(II) complexes are lowered uniformly by ~ 0.7 eV with respect to the analogous orbitals of (5,10,15,20-tetraphenylporphinato)-zinc(II) species,³⁷ significant charge resonance interactions in **5** may enforce a more coplanar ground-state structure than is manifest by **2** and **7**. While X-ray structural data to support this hypothesis are lacking, evidence bolstering this assertion can be gleaned from the cyclic voltammetric data obtained for these species: **2** and **7** show peak-to-peak potentiometric separations (ΔE_p values) for the initial cathodic steps of their respective first reductive processes of 145 mV, while the analogous redox process for **5** displays a ΔE_p value of 230 mV (Supporting Information), signaling a larger structural reorganization upon forming the radical anion state than accompanies the analogous reaction in the former species. Likewise, as charge resonance will also drive enhanced configuration interaction in **5** relative to **2** and **7**, the (porphinato)zinc(II)-localized LUMO-LUMO interactions displayed in Figure 7E-G may all contribute to description of **5**'s radical anion state and, thus, play a supplementary role in effecting net destabilization of **5**'s $E_{1/2} \text{PZn}^{-0}$ value relative to the $E_{1/2} \text{PZn}^{-0}$ potential determined for **11**.

Conclusion

This work demonstrates that sequential Pd-catalyzed cross-coupling and metal-templated [2+2+2] cycloaddition reactions define a powerful approach to modulate systematically the electronic structure of the cofacial bis[(porphinato)metal] structural motif; this unprecedented potentiometric engineering of face-to-face porphyrin structures derives from the fact that this synthetic method is amenable to porphyrinic building blocks of widely varying electronic structure and provides for the first time a straightforward approach to control the topological connectivity between the conjugated macrocycles. Structural highlights of this extensive series of new cofacial bis(porphyrin) species include the first examples of such complexes that feature β -to- β bridging motifs, as well as macrocycles that possess σ -electron-withdrawing perfluoroalkyl substituents.

Cyclic voltammetric studies show that the electrochemically determined HOMO and LUMO energy levels of these cofacial bis(porphinato)zinc(II) complexes can be lowered by 780 and 945 mV, respectively, relative to the archetypal members of this class of compounds (Figures 8 and 9);⁵⁴ importantly, these orbital energy levels can be modulated over well-defined increments throughout these wide potentiometric domains.

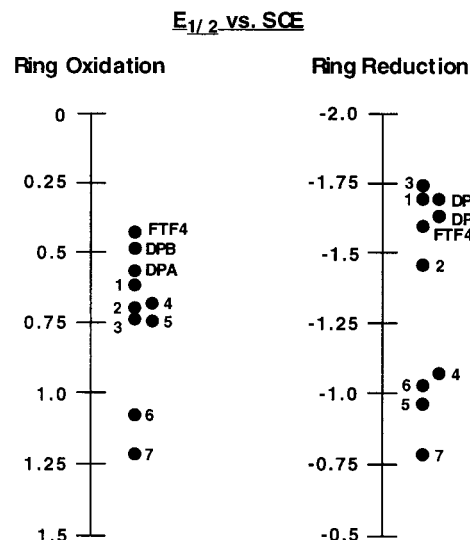


Figure 9. Redox potentials of the first oxidation ($E_{ox}(11)$ or $E_{ox}(1)$) and reduction ($E_{red}(11)$ or $E_{red}(1)$) processes of cofacial bis[(porphinato)zinc(II)] complexes vs SCE. The values for compounds FTF4, DPB, and DPA (Figure 8) are taken from ref 54.

Analyses of these cofacial bis[(porphinato)metal] potentiometric data, in terms of the absolute and relative frontier orbital energies of their constituent [porphinato]zinc(II) building blocks, as well as the nature of macrocycle-to-macrocycle connectivity, provide predictive electronic structural models that rationalize the redox behavior of these species. Importantly, this comprehensive data set emphasizes the importance of the relative phase relationships of the macrocycle-localized frontier orbitals in determining the electronic properties of face-to-face bis(porphyrin) compounds. As such, this investigation suggests a key refinement to the highly successful Hunter-Sanders model of arene-arene π - π interactions, which predicts the electronic structural properties of stacked aromatic assemblies through analysis of π -system charge distributions.

It is noteworthy that cofacial porphyrin constructs have shown utility as ligands for a wide range of transition-metal-catalyzed multielectron redox transformations of small-molecule substrates;¹² well-studied examples include multielectron oxygen^{1-6,8,10} and nitrogen⁹ reduction reactions, as well as water,^{7,13} hydrogen,^{11,15} and hydrocarbon¹⁵ oxidations. Perhaps the most remarkable aspect of these reactions is that the initial examples of each were all delineated with bimetallic catalysts possessing ligand frameworks having similar electronic structure.

A necessary consequence of utilizing similarly electron-rich porphyrin macrocycles in cofacial bis[(porphinato)metal] catalysts is the fact that these systems often operate at substantial overpotential with respect to the thermodynamic potential of the small-molecule multielectron redox conversion of interest.¹² As illustrated in Figure 9, through systematic augmentation of the number of σ -electron-withdrawing perfluoroalkyl substituents in the bis[(porphinato)metal] ligand framework, the cathodic and anodic potential domains can be tuned incrementally through approximate 1-V windows. Such potentiometric engineering defines an important tool to exploit in the development of new cofacial porphyrin redox catalysts that operate closer to the substrate thermodynamic potential. Finally, given that this report (i) defines archetypal examples of highly electronically asymmetric bis[(porphinato)metal] structures and (ii) shows that macrocycle-macrocycle lateral shift can be modulated via the

nature of the porphyrin–porphyrin topological connectivity, entirely new opportunities may evolve for the development of catalysts to effect heterolytic bond activation and subsequent multielectron redox transformations of dipolar small molecules.

Acknowledgment. This work was supported in part by the MRSEC Program of the National Science Foundation (DMR00-79909). M.J.T. acknowledges the Camille and Henry Dreyfus Foundations for a research fellowship. J.T.F. thanks the International Precious Metals Institute (IPMI) for a graduate student research award.

Supporting Information Available: Characterization data and detailed syntheses of halogenated and ethynyl-substituted trifluoromethylporphyrin precursor compounds, exemplary cyclic voltammetric responses for **2**, **6**, **7**, and **9–11**, computed cofacial porphyrin structures and tabulated data used to approximate interplanar separations, and qualitative depictions of HOMO and LUMO interactions occurring at van der Waals contact in cofacial porphyrin systems possessing fully coplanar orientations. This material is available free of charge via the Internet at <http://pubs.acs.org>. See any current masthead page for ordering information and Web access instructions.

JA012489H